Copper-functionalized nanostructured silica-based systems: Study of the antimicrobial applications and ROS generation against gram positive and gram negative bacteria

Diana Díaz-García [a], Perla R. Ardiles [b], Miguel Díaz-Sánchez [a], Irene Mena-Palomo [a], Isabel del Hierro [a], Sanjiv Prashar [a], Antonio Rodríguez-Diéguez [c], Paulina L. Páez [b,*] and Santiago Gómez-Ruiz [a,*]

[a] *Departamento de Biología y Geología, Física y Química Inorgánica, ESCET, Universidad Rey Juan Carlos, Calle Tulipán s/n, E-28933, Móstoles (Madrid), Spain.*

[b] *Departamento de Ciencias Farmacéuticas. Facultad de Ciencias Químicas, Universidad Nacional de Córdoba. Ciudad Universitaria, Haya de la Torre y Medina Allende, X5000HUA Córdoba, Argentina.*

[c] *Departamento de Química Inorgánica, C/ Severo Ochoa s/n, Universidad de Granada, 18071, Granada, Spain.*

* Corresponding authors: santiago.gomez@urjc.es (S.G.-R.) and plpaez@fcq.unc.edu.ar (P.L.P.)

Dedicated to the memory of our friend Prof. Juan Manuel Salas Peregrín and his pioneering research work on Bioinorganic Chemistry in Spain

Abstract

A series of copper-functionalized SBA-15 (Santa Barbara Amorphous) materials containing the ligands triethoxysilylpropylmaleamic acid (maleamic) or triethoxy-3-(2-imidazolin-1-yl)propylsilane (imidazoline) have been prepared. The nanostructured silica-based systems SBA-maleamic, SBA-imidazoline, SBA-maleamic-Cu and SBA-imidazoline-Cu were characterized by several methods observing that the functionalization took place mainly inside the pores of the mesoporous system. The antimicrobial behaviour of the synthesized materials against *Staphylococcus aureus* and *Escherichia coli* was tested observing a very potent activity of the copper-functionalized systems (minimum inhibitory concentration (MIC) and minimum bactericidal concentration (MBC) values for SBA-maleamic-Cu of ca. 31.25 μg/mL, which correspond

with ca. 1.13 μg/mL of Cu). A study of the oxidative stress promoted by the synthesized materials showed that the SBA-maleamic-Cu and the SBA-imidazoline-Cu were able to increase the reactive oxygen species (ROS) production in *S. aureus* by 427% and 373%, respectively, while this increase was slightly lower in *E. coli* (387 and 324%, respectively). Furthermore, an electrochemical study was carried out in order to determine if these materials interact with lysine or alanine to validate a potential antimicrobial mechanism based on the inhibition of the synthesis of the peptidoglycan of the bacterial wall. Finally, these studies were also performed to determine the potential interaction of the copper-containing materials with glutathione in order to assess if they are able to perturb the metabolism of this tripeptide.

Keywords: mesoporous silica; SBA-15; copper; antibacterial activity; ROS; electrochemistry

1. Introduction

Mesoporous silicas are an interesting class of materials in different fields of research, and which have become of high importance in science due to their attractive properties, such as a high surface area, tuneable pore size, particle size and morphology along with a very high chemical stability [1].

In a medicinal context, mesoporous silica have been studied in nanomedicine [2] as drug-delivery systems [3], loaded with several therapeutic agents such as metallodrugs of different metals, namely, platinum [4–7], titanium [4,8–15], tin [15–19], ruthenium [20] and copper compounds [21]. Mesoporous silica in drug-delivery has also been loaded with FDA-approved organic drugs [22,23] and even with natural products with therapeutic activity [24–26]. All these drug-delivery systems have shown interesting results in anticancer studies *in vitro* or *in vivo*, demonstrating their potential to be used in many other therapies such as, for example, cancer immunotherapy [27].

Bearing in mind that one of the most active research fields in medicinal chemistry is currently focused on the study of novel therapeutic approaches to fight against highly resistant bacteria [28], the use of mesoporous silica-based nanostructured systems as carriers of more potent antimicrobial agents represents an exploitable alternative [29]. Thus, the search for novel materials with potential antimicrobial activity in the first moments of microorganism colonization, which is critical in the propagation of the infection, is very intense [30]. The use of mesoporous silica-based materials loaded with

antibacterial agents has been traditionally restricted to commercial antibiotics [29–31] or other biocides [32,33]. However, few studies have been reported using mesoporous silica-supported metal-based antibacterial drugs or supported metal (mainly Cu or Ag) nanoparticles [34,35].

In this context, our group recently reported the preparation and study of the antibacterial properties of copper(II) maleamate complexes supported on mesoporous silica nanoparticles (MSN) [21]. Maleamates ligands were chosen because they have a rich coordination chemistry [36–40] and a very high potential to perturb the biological action of the enzyme maleamate amidohydrolase, negatively affecting the bacterial viability [41,42]. In addition, copper ions were used for the preparation of the metal complexes, as copper(II) compounds have a very long tradition in antibacterial studies, demonstrating a very high antimicrobial activity [43–45].

In view of our interesting results in this field which show that copper(II) maleamate complexes supported onto MSN exhibit excellent activity against *Staphylococcus aureus* and *Escherichia coli*, generating a high quantity of ROS and strongly decreasing bacterial viability [21]; we decided to continue our studies using copper(II) maleamate complexes supported on SBA-15 mesoporous silica, extending the work to the use of other ligands such as imidazoles, as this kind of organic ligands have already been shown to be active antibacterial agents [46–49].

Thus, in this study we have prepared and characterized two different SBA-15 based materials with supported copper(II) complexes containing silylpropylmaleamato or (2-imidazolin-1-yl)propylsilane ligands. In addition, a complete study of the antibacterial activity and ROS generation in *S. aureus* and *E. coli* colonies has also been carried out. An electrochemical study of the binding ability and interaction of these materials with lysine and glycine has been undertaken in order to determine if the supported copper(II) complexes interact in the peptidoglycan synthesis of the membrane of the bacteria [50]. Finally, an electrochemical binding study of the materials with glutathione has also been carried out, in order to observe if these materials have the potential to bind with glutathione perturbing the metabolism of this peptide, which may result in the promotion of an alternative cell death pathway for the bacteria.

2. Experimental Section

2.1. General remarks on the synthesis of the materials

All reactions were performed using standard Schlenk tube techniques in an atmosphere of dry nitrogen. Solvents were distilled from the appropriate drying agents and degassed before use. The reagents used in the preparation of the starting material (SBA-15),

poly(ethylene glycol)-block-poly(propylene glycol)-block-poly(ethylene glycol) (Pluronic 123) and tetraethyl orthosilicate (TEOS) were purchased from Sigma Aldrich. Triethoxysilylpropylmaleamic acid (maleamic) (Fluorochem), triethoxy-3-(2-imidazolin-1-yl)propylsilane (imidazoline) (Fluorochem), copper(II) nitrate trihydrate (Sigma-Aldrich) and 5,5'-dimethyl-2,2'-bipyridine (Fluorochem) and NaOH (Scharlau) were used for the preparation of the functionalized SBA-15 based materials. Finally, for the electrochemical study lysine (Fluorochem), glycine (Sigma-Aldrich) and glutathione (Sigma-Aldrich) were used. All reagents were employed directly without further purification.

2.2. General remarks on the characterization of the materials

X-ray diffraction (XRD) pattern of the systems were obtained on a Philips Diffractometer model PW3040/00 X'Pert MPD/MRD at 45 kV and 40 mA, using a wavelength Cu Kα (λ = 1.5418 Å). Cu wt% determination by X-ray fluorescence were carried out with an X-ray fluorescence spectrophotometer Philips MagiX with an X-ray source of 1 kW and a Rh anode using a helium atmosphere. Thermogravimetry analyses (TG) were obtained on a Shimadzu mod. DSC-50Q (Shimadzu, Kioto, Japan) operating at 950 ºC (ramp 20 ºC/min) at an intensity of 50 A. IR spectra were prepared using KBr pellets with a spectrophotometer Termo Nicolet Avatar 380 FT-IR with a Michelson filter interferometer. N_2 gas adsorption–desorption isotherms (BET) were performed using a Micromeritics ASAP 2020 analyzer. DR UV-Vis measurements were carried out on a Varian Cary-500 spectrophotometer equipped with an integrating sphere and polytetrafluoroethylene (PTFE) as reference. ^{13}C CP MAS NMR (^{13}C cross polarization magic angle spinning nuclear magnetic resonance) and ^{29}Si MAS NMR (^{29}Si magic angle spinning nuclear magnetic resonance) spectra, were recorded on a Varian-Infinity Plus Spectrometer at 400 MHz operating at 100.52 MHz proton frequency (4 μs 90° pulse, 4000 transients, spinning speed of 6 MHz, contact time 3 ms, pulse delay 1.5 s). Transmission electron microscopy (TEM) was carried out on a JEOL JEM 1010, operating at 100 kV and Nano scanning electron microscopy (nano-SEM) was carried out with a Nova NanoSEM 230, operating at 3 kV.

2.3. General remarks on the electrochemical studies

The cyclic voltammograms were recorded with a potentiostat / galvanostat Autolab PGSTAT302 Metrohm. A conventional three electrode system was used throughout the electrochemical experiments at room temperature with a modified carbon paste electrode (CPE) as the working electrode, a platinum wire as the auxiliary electrode, and a saturated Ag/AgCl/KCl (3 M) electrode (Metrohm) as the reference electrode against which all potentials were measured. The phosphate buffer used as the electrolyte

solution in the cell was purged with high purity nitrogen gas for at least 5 min to remove dissolved oxygen and then a nitrogen atmosphere was kept over the solution during measurements.

2.4. Synthesis of mesoporous silica nanoparticle (SBA)

The synthesis of SBA-15 was carried out from a modification of the experimental procedure reported by *D. Zhao et al*. [51]. In summary, an aqueous solution of the triblock copolymer Pluronic 123 (24.00 g, 4.14 mmol) was dissolved in 180 mL of Milli-Q water with ultrasound. Hydrochloric acid (720 mL, 2 M) was added to the solution and the temperature raised to 35 ºC. The silica precursor, TEOS (54.66 mL, 244.80 mmol), was added dropwise under vigorous stirring (1000 rpm) and the reaction allowed to proceed for 20 hours. Subsequently, the ageing process began. For that, the stirring was stopped and the mixture was heated to 80 ºC for 24 hours (under static conditions). The white precipitate was filtered and washed with abundant nanopure (Milli-Q) water. The solid was then dried for 24 hours at 80 ºC. Finally, a calcination process was carried out for 12 hours at 500 ºC with a temperature ramp of 1º C / minute.

2.5. Functionalization of SBA-maleamic

Firstly, SBA-15 (3.00 g) was dried under vacuum at 80 ºC for 24 h. The SBA-15 silica was then treated with a solution of triethoxysilylpropylmaleamic acid (6.00 g, 18.78 mmol) in 30 mL of dry toluene, and the solution was kept under stirring for 48 hours at 110 ºC. The suspension was then filtered and the isolated solid washed with toluene and diethyl ether (2 × 50 mL) and dried for 24 h at 80 ºC.

2.6. Functionalization of SBA-imidazoline

The synthesis of this material was carried out using the same synthetic method to that of SBA-maleamic. 3.00 g of SBA-15 was dispersed in 30 mL of dry toluene and a solution of triethoxy-3-(2-imidazolin-1-yl)propylsilane (5.97 mL, 21.86 mmol) in 20 mL of toluene was added to the suspension. The reaction was heated to 110 ºC and kept under stirring for 48 hours. The suspension was filtered and the isolated solid washed with toluene and diethylehter (2 × 50 mL) and then dried for 24 h at 80 ºC.

2.7. Synthesis of SBA-maleamic-Cu and SBA-imidazoline-Cu

The preparation of SBA-maleamic-Cu and SBA-imidazoline-Cu was carried out following similar procedures to those published by our group [21]. In summary, to a suspension of 0.85 g of SBA-maleamic or SBA-imidazoline in 20 mL of acetonitrile, 357 mg (1.48 mmol) of copper(II) nitrate trihydrate and 272.3 mg (1.48 mmol) of 5,5'-dimethyl-2,2'-bipyridine (the quantity of copper(II) nitrate was calculated to obtained a theoretical level of 10% Cu/SiO_2) was added. A solution of sodium hydroxide (5 mL, 2 % NaOH w/w with the

solution) was added and the reaction was maintained at 80 ºC for 24 h. The product was centrifuged (6000 rpm, 10 min.), washed and dried to eliminate the excess of reagents.

2.8. Antibacterial activity

The minimum inhibitory concentration (MIC) and the minimum bactericidal concentration (MBC) of the copper complex were determined in *S. aureus* ATCC 29213 and *E. coli* ATCC 25922 according to methods standardized by the Clinical and Laboratory Standards Institute [52]. The inoculum was prepared from an overnight culture with a cell concentration 1-5 × 10^8 colony forming units per/mL (CFU/mL) corresponding to 0.5 in McFarland scale. It was then diluted 1:100 in Mueller Hinton medium. Serial dilutions from 250 to 0.125 μg/mL of each compound were made in a 96-well microplate. Then, the inoculum, to a concentration of 1-5 × 10^6 CFU/mL, was added and the culture microplates were incubated at 37 °C for 48 h. MIC was defined as the lowest concentration of the compounds without visible microbial growth after 18 h of incubation. The antimicrobial agent concentration that produces the death of 99.9% of initial inoculum was considered as the MBC.

2.9. Determination of Reactive Oxygen Species

A bacterial suspension (100 µL) of *S. aureus* ATCC 29213 and *E. coli* ATCC 25922 was incubated with 100 µL of the each compound at MIC concentration for 1 h at 37 °C. Then, 20 µL of H_2-DCFDA 20 µM aqueous solution (Cellular ROS Assay Kit) was added. The fluorescence intensity was measured 30 min later with a spectrofluorometer Biotek Synergy HT with the excitation and emission wavelengths at 480 and 520 nm, respectively. Non-treated bacterial suspensions were used as the control. The experiments were carried out in triplicate.

2.10. Electrode Preparation

Cyclic voltammetry (CV) and differential pulse voltammetry (DPV) measurements have been performed and the experiments have been carried out at room temperature, using a three-electrode-single compartment electrochemical cell (100 mL and dimensions of 7.5 cm high and 6.5 cm diameter) with a Ag/AgCl/KCl 3 M as the reference electrode and a platinum rod counter electrode. A modified carbon paste with SBA-functionalized materials was used as the working electrode. The modified carbon paste electrodes (MCPE) used as working electrode were prepared by mixing with a pestle in an agate mortar the previously modified mesoporous materials with graphite (Metrohm) (6-10% (wt,wt) ratio) and mineral oil as agglutinant (Sigma-Aldrich) until a uniform paste was obtained. The resulting material was packed into the end of a Teflon cylindrical tube equipped with a screwing stainless steel piston providing an inner electrical contact. All

of the initial electrode activity could always be restored by simply removing the outer layer of paste by treatment with polishing paper. DPV parameters were as follows: the initial potential of -1.0 V, the end potential -1.75 or -2.0 V, the modulation time 0.057 s, the time interval 0.2 s, the step potential 1.05 mV/s, the modulation amplitude of 75 mV.

3. Results and Discussion

3.1. Synthesis and characterization of SBA-15 mesoporous silica

The preparation of SBA-15 was carried out using the method described previously by Zhao and coworkers [51]. This method is based on the use of Pluronic 123 as surfactant and TEOS as silicon source in an acidic medium. A subsequent ageing process of 24 hours under static conditions at 80 ºC and a final calcination step at 500 ºC, leads to the preparation of mesoporous silica SBA-15. The solid obtained was characterized by several methods to determine various important features of the material such as particle morphology and size, pore size and mesoscopic order.

The analysis of the SBA-15 by low angle powder XRD studies showed that this material gave three diffraction peaks (Figure 1) corresponding with an hexagonally ordered silica. Namely, an intense peak associated with the (100) Miller plane was observed at 2θ of 1.00, while two low intensity peaks were observed at 2θ of 1.68 and 1.95, which were assigned to the (110) and (200) Miller planes of the SBA-15 (Table 1).

SBA-15 was also characterized by nitrogen sorption studies, observing type IV isotherms (according to the IUPAC classification) [53], with an hysteresis loop H2b (Figure 2) which is associated with the typical process of capillary condensation of mesoporous materials [53]. The BET surface area for this material is 763 m^2/g, the total pore volume ca. 0.74 cm^3/g and the pore diameter 6.55 nm (Table 2). These data confirm the mesoporous nature of the synthesized SBA-15 material and are in agreement with other previously synthesized unmodified SBA-15 materials [15–19,51].

Characterization by ^{29}Si MAS NMR spectroscopy gave a spectrum showing the signals corresponding to the different silicon atoms of the silica structure with hydroxyl bound groups, namely [$Si(OSi)_2$] (the most intense peak (Q^4) which appears at -112.7 ppm), [$Si(OSi)_2(OH)$] (a very intense peak (Q^3) which is observed at -105.3 ppm), [$Si(OSi)_2(OH)_2$] (a low intensity peak (Q^2) which is found at -95.3 ppm), and finally [$Si(OSi)(OH)_3$] (Q^1, which is of very low intensity and appears at -86.2 ppm). The very high intensity of the peaks Q^4 and Q^3 confirms the mesoporous nature of the synthesized SBA-15 material [54].

SBA-15 was characterized by SEM and TEM (Figure 3). The synthesized SBA-15 can be defined as nanostructured rods of ca. 1.3 μm long and around 500 nm wide with a

narrow distribution of the particle size. In addition, the TEM micrographs show the parallel pore channels distribution along the particles.

3.2. Synthesis and characterization of functionalized SBA-15 materials

The synthesized SBA-15 was functionalized with two different ligands, namely, triethoxysilylpropylmaleamic acid (maleamic) and triethoxy-3-(2-imidazolin-1-yl)propylsilane (imidazoline) to yield SBA-maleamic and SBA-imidazoline, respectively (Scheme 1). Both grafting reactions were carried out in toluene at 110 ºC for 48 hours and led to protonolysis of the Si-OH groups and elimination of ethanol from the ligands leading to new ligand containing Si-O-Si fragments.

Subsequently the materials SBA-maleamic and SBA-imidazoline were treated with an acetonitrile solution of copper(II) nitrate in the presence of both sodium hydroxide and 5,5'-dimethyl-2,2'-bipyridine, to give the materials SBA-maleamic-Cu and SBA-imidazoline-Cu, where the maleamic and the imidazoline ligands, respectively, are coordinated to a copper(II) ion as shown in Scheme 2.

All materials were characterized by a variety of the typical techniques employed in solid-state chemistry. Thus, for example, the powder XRD studies showed that after functionalization with either maleamic ligand, imidazoline ligand or copper, the diffraction peaks appear with much lower intensity compared to those of the unmodified SBA-15 (Figure 1 for maleamic-based materials and Figure S1 of Supplementary Material for imidazoline-based materials). The decrease in the intensity is associated with the partial blocking of the dispersion centres (pores) of the mesoporous material after functionalization with the ligands and / or the copper-containing moiety. A similar effect has been found in several other systems described in the literature for metallodrug-functionalized SBA-15 materials [8,15–17] and is indicative of functionalization of the materials inside the pores of the mesoporous structure. In addition, the diffraction pattern of the functionalized materials, SBA-maleamic, SBA-imidazoline, SBA-maleamic-Cu and SBA-imidazoline-Cu, showed the typical signals at similar 2θ positions to those in the case of the unmodified SBA-15, confirming that the hexagonal mesoporous arrangement and the structural order of the materials are maintained unaltered.

The nitrogen sorption study (Table 2 and Figure 2) showed that the BET surface area (S_{BET}) of the copper-functionalized materials SBA-maleamic-Cu and SBA-imidazoline-Cu were of 150 and 142 m^2/g, respectively. The dramatic decrease in the surface area of the functionalized system when comparing with the unmodified SBA-15 (763 m^2/g) is due to the functionalization with the copper complex inside the pores of the system. In addition, the functionalization inside the pores of the mesoporous system is also patent

when comparing the BJH (Barnett, Joyner and Halenda) pore size of the materials. Thus, SBA-maleamic-Cu and SBA-imidazoline-Cu have pore diameters of 3.15 and 4.71 nm, respectively, which are much lower than that of the unmodified SBA-15 which has a value of 6.55 nm. It is important to note that capillary condensation of nitrogen within the uniform mesoporous structure occurred for all the studied materials. This is observed at relative pressures (P/P_0) of ca. 0.3 for SBA-maleamic-Cu and SBA-imidazoline-Cu and at ca. 0.4. The decrease in the relative pressure for SBA-maleamic-Cu and SBA-imidazoline-Cu compared with that of SBA-15 is an effect of the functionalization.

The copper containing materials were also characterized by XRF in order to determine the quantity of Cu of both SBA-maleamic-Cu and SBA-imidazoline-Cu. The quantity of Cu found was 3.6 % wt for SBA-maleamic-Cu and 12.3 % wt. for SBA-imidazoline-Cu (Table 2), which correspond to a functionalization of 0.56 and 1.94 mmol/gram of material for SBA-maleamic-Cu and SBA-imidazoline-Cu, respectively.

The characterization of the functionalized materials SBA-maleamic, SBA-maleamic-Cu, SBA-imidazoline and SBA-imidazoline-Cu by ^{29}Si MAS NMR spectroscopy confirmed the immobilization of the ligands and the copper complex. In the ^{29}Si MAS NMR spectra of SBA-maleamic, SBA-maleamic-Cu, SBA-imidazoline and SBA-imidazoline-Cu the signals associated with the Q^4, Q^3, Q^2 peaks of the silica were observed as in the case of the spectrum of the unmodified SBA-15 (in all cases the chemical shift of the signals was very similar, Figure 4). However, the intensity of the Q^4 and Q^3 peaks decreased for SBA-maleamic, SBA-maleamic-Cu, SBA-imidazoline and SBA-imidazoline-Cu when compared with the spectrum of unmodified SBA-15. In addition, the ^{29}Si MAS NMR spectra of the functionalized materials showed two new peaks of medium intensity and at ca. -69 and -62 ppm, corresponding to the T^2 ($(SiO)_2SiOH–R$) and T^3 ($(SiO)_3Si–R$) sites, respectively, which confirm the incorporation of the maleamic or imidazoline ligand via elimination of two or three ethanol groups and the formation of the corresponding Si-O-Si bonds.

The materials SBA-maleamic-Cu and SBA-imidazoline-Cu were also characterized by ^{13}C CP MAS NMR spectroscopy. In the case of SBA-maleamic-Cu the ^{13}C CP MAS NMR spectrum (Figure 5) shows the typical signals associated with the propylsilylmaleamate ligand and the ethoxide groups, namely, the signals of the $Si–CH_2–CH_2–CH_2–N$ fragment were observed at ca. 12, 21 and 54 ppm. The maleamate ligand gave two additional broad signals at ca. 125-140 ppm which are due to the alkenylic carbon atoms of the maleamate. In addition, the carbon atoms of the dimethylbipyridine ligand appeared as a very broad signal at ca. 174 ppm (aromatic carbons of the bipyridine) and a signal at ca. 40 ppm, due to the carbon atoms of the methyl groups bound to the aromatic rings.

It is important to note that the signals of the carbon atoms of the COO and CONH moiety of the maleamate ligand were not easily observed and appear with very low intensity between 200 and 205 ppm. Finally, the signals associated with the pendant ethoxide groups were observed in the spectrum at ca. 60 ppm (OCH_2) and 33 ppm (CH_3).

For SBA-maleamic-Cu, the ^{13}C CP MAS NMR spectrum shows a set of signals which confirm the incorporation of the imidazoline ligand. Thus, the three typical signals of the Si–CH_2–CH_2–CH_2–N fragment were observed between 8 and 55 ppm. In addition, in the same region, two additional signals corresponding to the sp^3 carbon atoms of the imidazole ring were also observed. The spectrum also shows a broad signal between 120 and 130 ppm which is due to the sp^2 carbon atom of the imidazole ring. Furthermore, the carbon atoms of the dimethylbipyridine ligand were observed as a broad signal at around 160 ppm (aromatic carbons of the bipyridine) and a signal at ca. 40 ppm, due to the carbon atoms of the methyl groups bound to the aromatic rings. Finally, the signals associated with the pendant ethoxide groups were recorded at ca. 60 ppm (OCH_2) and 22 ppm (CH_3).

The functionalized materials SBA-maleamic, SBA-maleamic-Cu, SBA-imidazoline and SBA-imidazoline-Cu have also been characterized by DR-UV-vis spectroscopy (Figure 6). The spectra of both SBA-maleamic, SBA-maleamic-Cu show an intense absorption peak at ca. 220 nm and a absorption shoulder at ca. 260 nm, due to the maleamic ligand. In addition, only the spectrum of SBA-maleamic-Cu (which includes the incorporation of copper nitrate and the coordination of bipyridine) shows an additional absorption band at ca. 307 nm which is due to metal to ligand charge transfer (MLCT), indicating coordination. DR-UV spectra of both SBA-imidazoline, SBA-imidazoline-Cu gave a very intense absorption peak at ca. 205 nm and a low intensity absorption shoulder at ca. 250 nm (more pronounced in the spectrum of SBA-imidazoline-Cu), due to the imidazoline ligand. In addition, only the spectrum of SBA-imidazoline-Cu shows an intense absorption peak at ca. 312 nm due to metal to ligand charge transfer, confirming the coordination of the imidazoline ligand to copper.

All the synthesized materials were characterized by FT-IR spectroscopy observing the appearance of the typical peaks of each of the supported compounds (maleamic, imidazoline and copper moieties) and which confirms the functionalization of SBA-15-based materials (See Figure S2 of Supplementary Material).

Furthermore, materials SBA-15-maleamic-Cu and SBA-15-imidazoline-Cu were also characterized by SEM (Figure 7) observing no significant changes in the morphology and particle size of the functionalized materials. An EDX mapping of a SEM image of

SBA-imidazoline-Cu was carried out to show the distribution of Si, O and Cu atoms in the external surface area of the material (Figure 8). One can easily see that the quantity of Cu seems to be very low, which is in agreement with the fact that the major functionalization of the material is inside the pores of the mesoporous silica particles (not easily visible in SEM) together with the relatively low quantity of Cu (12.3 % wt. XRF) present in the whole material.

Finally, materials SBA-15-maleamic-Cu and SBA-15-imidazoline-Cu were also characterized by TEM (Figure 9), observing that the pore arrangement of the functionalized materials is retained.

3.3. Antibacterial studies of functionalized SBA materials

To evaluate the efficacy of the synthesized copper-functionalized materials as antibacterial agents, the MIC and MBC of SBA-15, SBA-maleamic, SBA-maleamic-Cu, SBA-imidazoline and SBA-imidazoline-Cu were determined against *S. aureus* and *E. coli* (Table 3).

The results showed that SBA-15 did not exhibit any antibacterial effect up to 250 µg/mL against *S. aureus* and *E. coli*, while the functionalized materials showed bactericidal activity against both bacteria (MBC/MIC< 2). MIC and MBC values obtained with SBA-maleamic-Cu (31.25 µg/mL of material or 1.13 µg/mL of Cu) were lower, and therefore more interesting, than those obtained from SBA-maleamic (125 µg/mL) indicating that the functionalization of the materials with copper ions leads to a significant increase in the antibacterial properties, up to four times in both *S. aureus* and *E. coli*. However, the effect of the incorporation of copper on the antibacterial potential of SBA-imidazoline-Cu was lower as the MBC of SBA-imidazoline and SBA-imidazoline-Cu is the same while the decrease of MIC of SBA-imidazoline-Cu compared with that of SBA-imidazoline was 50%.

The antibacterial activity of these materials is much higher than that found for similar systems published previously by our group and based on MSN materials [21] and comparable, if not somewhat better than those obtained by Wang et al with tannic acid-loaded mesoporous silica nanoparticles [55]. In general, when compared with other metal complexes [56], the copper-functionalized systems described here present a much higher bactericidal activity (referred to metal dose, which for these materials is between 1.13 and 15.38 µg/mL) than several metal complexes against *S. aureus* and *E. coli*. In addition, the copper-containing materials present higher antibacterial activity than some commercial antibiotics [57,58].

3.4. Determination of ROS promoted by functionalized SBA materials

Oxidative stress is caused by a high intracellular concentration of reactive oxygen species (ROS) [59]. ROS usually promote the oxidation of some essential macromolecules inside the cells and leads to cell death by triggering different mechanisms [60]. In this context, the determination of oxidative stress is appropriate to elucidate if this is the principal cause of the antibacterial effect of the antibiotic agents.

Thus, the production of ROS was determined for the synthesized materials. SBA-15, SBA-maleamic, SBA-maleamic-Cu, SBA-imidazoline and SBA-imidazoline-Cu in bacterial suspensions were incubated at 37 ºC during 1 hour with a dose of 100 µL of the synthesized materials at the determined MIC concentration (Figure 10). The materials were able to stimulate the generation of ROS in *S. aureus* and *E. coli*. The highest increase in ROS was obtained with SBA-maleamic-Cu in both studied strains. Interestingly, the increase in ROS with the studied materials was lower in *E. coli* than in *S. aureus*, in contrary to that found for other copper-containing silica-based materials reported by our group [21]. This indicates that the type of material (MSN or SBA-15) has an influence on the ROS production in bacteria. It is important to note that, for the case of copper-functionalized materials the increase of ROS generation is higher than their analogues functionalized only with the ligands maleamic or imidazoline. Of special importance is the capacity of ROS generation of the material SBA-maleamic-Cu, which is able to increase ROS production in *S. aureus* to 427% and in *E. coli* to 387% with respect to the control. The capacity of ROS generation by SBA-imidazoline-Cu is slightly lower with values of 373% and 324% in *S. aureus* and *E. coli*, respectively. When compared with similar systems based on MSN [21], the materials reported here increase the ROS production by almost three times. The ROS production might be a consequence of an electrochemical process mediated by Cu(II)/Cu(I) ions, as the potential reduction of the metal centre may induce the formation of oxidative species. A similar behavior for copper(II) complexes was recently reported by other authors, confirming the ability of copper(II) centres to get reduced to copper(I) leading to generation and dismutation of superoxide radicals resulting in an increase of ROS [61–63]. However, this might not be the only reason for the generation of ROS. When analyzing the photoluminescence spectrum of the most active material SBA-maleamic-Cu, a low intensity emission peak was found at 361 nm (See Figure S3 of supplementary material). Thus, one cannot completely rule out a photophysical process as a potential inductor of part of the ROS production of the copper-functionalized nanostructured systems.

3.5. Electrochemical binding study of Cu-functionalized materials with biomolecules of interest

Even though the results obtained in the ROS generation studies seem to point towards a bactericidal mechanism based on oxidative stress induction, additional electrochemical studies were carried out in order to determine if the synthesized materials are able to bind with lysine or alanine as these are aminoacids implicated in the peptidoglycan synthesis of the bacterial membrane [64].

Furthermore, our electrochemical study was also extended to glutathione, because the perturbation of the metabolism of this tripeptide in different bacteria may lead to its death [65–67]. Combination antibacterial therapy based on antibiotic and exogenous glutathione administration is an alternative current approach for treating bacterial infections [68–70].

In this context, we initially studied, by electrochemical methods, the binding behaviour of the most active material SBA-maleamic-Cu with alanine, lysine and glutathione, to determine if these materials bind to the molecules and have the potential to interact or inhibit the peptidoglycan synthesis and / or the glutathione bacterial metabolism. Thus, we designed a set of experiments to gain insights into the transportation processes and binding behaviour of copper complexes grafted onto hybrid mesoporous silica nanoparticles. This study has been undertaken by mimicking physiological media and studying the interaction of copper-functionalized silica-based materials with lysine and alanine and glutathione by means of solid state voltammetry techniques.

Taking into account the previous studies on this topic, in this section, electrochemical biosensor techniques have been employed in the investigation of drug-biomolecule interactions, cyclic voltammetry (CV) and differential pulse voltammetry (DPV) measurements have been performed and the experiments have been carried out at room temperature, using a three-electrode-single compartment electrochemical cell with a modified carbon paste as the working electrode, a Ag/AgCl/KCl 3 M the reference electrode and a platinum rod counter electrode. A modified carbon paste with SBA-functionalized materials has been used as the working electrode.

The first part of the electrochemical study was focused on the characterization of the material SBA-maleamic-Cu. Thus, CV was recorded for SBA-maleamic-Cu in the limits imposed by the solvent (Figure 11). When scanning from +1.0 to -1.5 V only one signal was observed at -1.06 V (vs Ag/AgCl) without any associated signal in the reversed scan. This irreversible redox process was attributed to the two electron reduction of Cu(II) coordinated simultaneously to maleamic ligand and bipyridine (and tethered to the silica

surface) to give Cu(0). It is important to note that electrochemical studies performed by Farias and co-workers [71] for salen-Cu(II) complexes in solution with a controlled growing mercury electrode (CGME) and in a buffer phosphate electrolyte medium showed several current peaks attributed, among others, to the quasireversible reduction process of Cu(II) to Cu(I) at -0.53 V and to the irreversible reduction of Cu(I) to Cu(0) at -1.0 V s. In addition, Mureseanu and coworkers [72] have designed a carbon paste electrode modified with mesoporous silica functionalized with the tripeptide Gly-Gly-His for copper (II) quantitative determination in aqueous media. When measuring the CV of Cu (II) solutions in Britton Robinson buffer, they observed a clear influence of the pH in the Cu(II)/Cu(0) redox couple, concluding that the current intensity decreases with increasing values of pH and that this signal is poorly defined at pH 7. These examples give evidence of the difficulty in comparing the redox processes attributed to copper complexes due to the different electrolyte, working electrode, pH, etc. used in the experiments.

In order to investigate the electrochemical properties of the tethered copper complex, we studied the influence of the scan speed. The cathodic peak current linearly increases on increasing the scan rate and the position of the peak slightly shifts towards more negative potentials. A linear variation of peak current with square root of scan rate is observed ($I_{red} = -5.10^{-7}-5.10^{-7}(v^{1/2})$ $R^2 = 0.9906$) suggesting that the process is diffusion controlled, in this case, by the counter ion diffusion, since the reduction process of copper requires a charge balance by an electrolyte cation.

This behaviour was confirmed by differential pulse voltammetry. Figure 12 shows the voltammogram recorded immediately after the immersion in the aqueous buffer phosphate electrolyte solution. As observed, one cathodic peak at -1.06 V assigned to the reduction of the copper complex attached to the silica surface appeared in the voltammogram. This peak remains constant in the timescale used in the experiments, suggesting the stability of the supported copper-maleamic-bipyridine complex in aqueous media. When the electroactivity of the material without copper SBA-maleamic is measured by cyclic voltammetry and differential pulse voltammetry, any comparable signals are observed in the limits imposed by the reduction of the solvent (See Figure S4 of supplementary material).

Once the electrochemical behaviour of the material SBA-maleamic-Cu in physiologic media was analyzed, the second part of the electrochemical study was focused on the determination of the binding behaviour as the use of electrochemical techniques in the study of metallodrugs-biomolecules interactions is very interesting due to the resemblance between electrochemical and biological reactions. The electrochemical

methods are extremely sensitive and are mainly based on the differences in the redox behaviour of the binding molecules in the absence and presence of target molecules including the shifts of the formal potential of the redox couple and the decrease of the peak current resulting from the dramatic decrease in the diffusion coefficient after association with the molecule under study in solution phase.

Firstly, differential pulse voltammetry measurements were used to study the binding ability of immobilized copper complexes towards the aminoacids lysine and alanine and the peptide glutathione as models of target molecules for the copper containing materials inside the cells.

Figure 12A shows the DPV recorded as a function of time of the modified carbon paste electrode with SBA-maleamic-Cu in the presence of a solution of lysine 4.0 mM in buffer phosphate at pH 7.4 as electrolyte. As observed in the voltammograms, in the presence of lysine 4.0 mM a new peak at -1.12 V appeared immediately after immersion of the electrode into the amino acid buffered solution. This new peak is shifted to lower potential values in comparison to that of SBA-maleamic-Cu and shows lower peak current intensity. This signal does not decrease with time, instead, it reaches a constant peak current immediately after contact with the electrode surface of the highly concentrated solution of lysine used in this essay, suggesting the formation of a copper-lysine adduct and the saturation of the copper active sites. After 10 minutes of the adsorption experiment, the copper-modified carbon paste electrode was removed from the lysine solution and the surface thoroughly washed with ultrapure water. A new measurement by using pure buffer phosphate as electrolyte showed that the initial signal at -1.06 V was not restored, instead, a much less intense peak and new additional signals at much more positive potentials appeared, suggesting the existence of copper leaching processes from the silica surface to the solution.

Since the initial activity of the electrode surface could not be restored after washing the surface, we decided to study the dependence of the influence of lysine-material with the concentration in terms of % of copper peak height change calculated by Equation 1. Due to the time dependent behaviour of the signals at lower lysine concentration values, a constant preconcentration time of 5 minutes was chosen to guarantee the formation of a potential SBA-maleamic-Cu···Lysine adduct under all concentration values used in the study.

$$\%\text{Interaction} = \frac{I_{complex-drug} - I_{complex}}{I_{complex}} \times 100 \qquad \text{(Eq. 1)}$$

As recorded in Table 3, the amount of lysine in solution showed a clear influence on the copper reduction peak height, that is, there is a decrease in the copper current peak on increasing the concentration of lysine in solution within the concentration range of 0.5 to 2.0 mM. At concentrations higher than 2.0 mM, the interaction Cu-lysine at the electrode surface is limited by the saturation of the metal active sites.

A very similar tendency to that observed above for lysine was observed when considering the effect of concentration of alanine and glutathione. The current peak decrease is more important with more concentrated solutions of the biomolecules (See Figure 12B and Figure 12C, and Figures S5 and S6 of supplementary material).

In the same manner a study was conducted for alanine and the peptide glutathione. The material SBA-maleamic-Cu showed a significant shift of the potential value from -1.06 V to -1.10 V in the presence of alanine 2 mM, which indicates the formation of a stable adduct. At similar glutathione concentration the observed shift is nearly negligible. In previous studies, as suggested by Melendez and co-workers, equation 2 was used to estimate, in a semiquantitative manner, the interaction between the metal complex and the target molecule, since the potential is more sensitive to the coordination environment than current [73–75].

$$\%\text{Interaction} = \frac{\text{E}_{\text{complex-drug}} - \text{E}_{\text{complex}}}{\text{E}_{\text{complex}}} \times 100 \qquad \text{(Eq. 2)}$$

As recorded in Table 4 the calculated interaction % based on potential peak change is higher for both aminoacids than that found for the tripeptide glutathione. When comparing both aminoacids lysine and alanine, the interaction % is slightly higher for lysine in all the studied concentration range. This behaviour can be explained in terms of copper complex stability, as the binding constant values found in previous reports for copper complexes follow the order $[Cu(Lys)_2]$ (log β) $\geq$ $[Cu(Ala)_2]$ (log β) > $[Cu(bipy)_3]$ (log K_1), which supports the fact that a ligand exchange reaction may take place [76–79], leading to decoordination of bipyridine and formation of $[Cu(aminoacid)_2]$ soluble species (Scheme 4). Furthermore, in the case of glutathione one can imagine that the higher steric hindrance imposed by this tripeptide is the reason for a significant lower interaction value with the copper-containing material SBA-maleamic-Cu (Table 4).

The proposed decoordination of bipyridine and formation of the soluble copper complexes would also validate the impossibility of restoring the signal of Cu(II) found

after removal of the copper-modified carbon paste electrode from the aminoacid or peptide solution and surface washing, because a leaching of Cu(II) ions occurs during the interaction studies (Scheme 4).

4. Conclusions

In conclusion, two different copper-functionalized SBA-15-based materials containing the ligands triethoxysilylpropylmaleamic acid (maleamic) or triethoxy-3-(2-imidazolin-1-yl)propylsilane (imidazoline) have been synthesized and characterized by a wide variety of methods observing that in both cases the functionalization with the copper complex takes place mainly inside the pores of the mesoporous system. Interestingly the material SBA-maleamic-Cu contains a much lower quantity of copper of ca. 3.6 %, while the system based on the imidazoline ligand had a much higher functionalization of ca. 12.3%.

The antimicrobial activity of all the synthesized materials was studied against *S. aureus* and *E. coli*, observing that, in spite of the lower quantity of copper, the material SBA-maleamic-Cu (MIC and MBC values for SBA-maleamic-Cu of ca. 31.25 μg/mL, which correspond with ca. 1.13 μg/mL of Cu) has a higher antibacterial activity than its analogue SBA-imidazoline. The antibacterial properties of the studied materials seem to come from the promotion of a high oxidative stress, as the materials SBA-maleamic-Cu and the SBA-imidazoline-Cu were able to increase the ROS production in *S. aureus* by ca. 4 times, respectively, while the increase was slightly lower in *E. coli*. The ROS generation appears to come from electrochemical processes associated with copper, rather than from a photophysical activation with light.

In spite of the fact that the ROS generation studies seem to point towards a bactericidal mechanism based on oxidative stress induction, additional electrochemical studies showed a high binding ability to lysine and alanine, which led to the leaching of the copper metal centres to the physiologic medium, presumably by formation of [Cu(aminoacid)$_2$] species, confirming the potential ability of these materials to interfere in the peptidoglycan synthesis as an alternative antibacterial mechanism. Finally, the binding ability of the system was tested with glutathione, observing a much lower binding capacity compared with that of alanine or lysine, indicating, therefore, a low potential of the material SBA-maleamic-Cu to interfere in the glutathione metabolism inside the bacteria.

Thus, the current efforts of our research team will be focused on determining the most attractive ligands and copper complexes to enhance and improve antimicrobial

properties against different bacterial colonies and biofilms, with the final goal of obtaining more effective materials which can overcome the problems of bacterial resistance critical for future antibacterial therapies.

Table of Abbreviations

ATCC - American Type Culture Collection

BET - Brunauer–Emmett–Teller

BJH – Barrett, Joyner and Halenda

CGME - Controlled growing mercury electrode

CP – Cross polarization

CPE – Carbon paste electrode

DCFDA - 2',7'–dichlorofluorescin diacetate

DPV – differential pulse voltammetry

DR-UV – Diffuse reflectance Ultraviolet

FDA – Food and Drug Administration

Imidazoline – triethoxy-3-(2-imidazolin-1-yl)propylsilane (imidazoline)

IUPAC – International Union of Pure and Applied Chemistry

Maleamic – triethoxysilylpropylmaleamic acid

MAS – Magic Angle Spinning

MBC - Minimum Bactericidal Concentration

MCPE – Modified Carbon Paste Electrode

MIC - minimum inhibitory concentration

MSN – Mesoporous Silica Nanoparticles

NMR – Nuclear Magnetic Resonance

PTFE - Polytetrafluoroethylene

ROS – Reactive Oxygen Species

SBA – Santa Barbara Amorphous

SEM – Scanning Electron Microscope

TEM – Transmission Electron Microscope

TEOS – Tetraethylorthosilicate

TG – Thermogravimmetry

UV – Ultraviolet

XRD – X-ray diffraction

XRF – X-ray fluorescence

Acknowledgements

We would like to thank the funding by the Ministerio de Ciencia, Innovación y Universidades Spain (grants numbers RTI2018-094322-B-I00 and CTQ2017-90802-REDT) and the Agencia Nacional de Promoción Científica y Tecnológica (ANPCyT) (PICT 2015 N 1558). We would also like to thank the Consejo Nacional de Investigaciones Científicas y Técnicas de Argentina (CONICET) and Dirección General de Investigación e Innovación, Consejería de Educación e Investigación de la Comunidad de Madrid for the predoctoral grants PEJD-2017-PRE/BMD-3512 (I. M.-P.) and PEJD-2017-PRE/AMB-4047 (M. D.-S.).

References

[1] R. Narayan, U.Y. Nayak, A.M. Raichur, S. Garg, Mesoporous Silica Nanoparticles: A Comprehensive Review on Synthesis and Recent Advances, Pharmaceutics. 10 (2018) 118. https://doi.org/10.3390/pharmaceutics10030118.

[2] M. Manzano, M. Vallet-Regí, Mesoporous silica nanoparticles in nanomedicine applications, J Mater Sci: Mater Med. 29 (2018) 65. https://doi.org/10.1007/s10856-018-6069-x.

[3] M. Vallet-Regí, M. Colilla, I. Izquierdo-Barba, M. Manzano, M. Vallet-Regí, M. Colilla, I. Izquierdo-Barba, M. Manzano, Mesoporous Silica Nanoparticles for Drug Delivery: Current Insights, Molecules. 23 (2017) 47. https://doi.org/10.3390/molecules23010047.

[4] W.A. Wani, S. Prashar, S. Shreaz, S. Gómez-Ruiz, Nanostructured materials functionalized with metal complexes: In search of alternatives for administering anticancer metallodrugs, Coordination Chemistry Reviews. 312 (2016) 67–98. https://doi.org/10.1016/j.ccr.2016.01.001.

[5] Y. Zheng, C.D. Fahrenholtz, C.L. Hackett, S. Ding, C.S. Day, R. Dhall, G.S. Marrs, M.D. Gross, R. Singh, U. Bierbach, Large-Pore Functionalized Mesoporous Silica Nanoparticles as Drug Delivery Vector for a Highly Cytotoxic Hybrid Platinum–Acridine Anticancer Agent, Chemistry – A European Journal. 23 (2017) 3386–3397. https://doi.org/10.1002/chem.201604868.

[6] I. del Hierro, Y. Pérez, P. Cruz, R. Juárez, Pt and Ti Complexes Immobilized onto Mesoporous Silica Microspheres and Their Interaction with Molecules of Biological Interest, European Journal of Inorganic Chemistry. 2017 (2017) 3030–3039. https://doi.org/10.1002/ejic.201700235.

[7] D. Edeler, M.R. Kaluderovic, B. Dojcinovic, H. Schmidt, G.N. Kaluderovic, SBA-15 mesoporous silica particles loaded with cisplatin induce senescence in B16F10 cells, RSC Adv. 6 (2016) 111031–111040. https://doi.org/10.1039/c6ra22596a.

[8] D. Pérez-Quintanilla, S. Gómez-Ruiz, Ž. Žižak, I. Sierra, S. Prashar, I. del Hierro, M. Fajardo, Z.D. Juranić, G.N. Kaluđerović, A New Generation of Anticancer Drugs: Mesoporous Materials Modified with Titanocene Complexes, Chemistry – A European Journal. 15 (2009) 5588–5597. https://doi.org/10.1002/chem.200900151.

[9] G.N. Kaluđerović, D. Pérez-Quintanilla, I. Sierra, S. Prashar, I. del Hierro, Ž. Žižak, Z.D. Juranić, M. Fajardo, S. Gómez-Ruiz, Study of the influence of the metal complex on the cytotoxic activity of titanocene-functionalized mesoporous materials, J. Mater. Chem. 20 (2010) 806–814. https://doi.org/10.1039/B919269G.

[10] G.N. Kaluderović, D. Pérez-Quintanilla, Z. Zizak, Z.D. Juranić, S. Gómez-Ruiz, Improvement of cytotoxicity of titanocene-functionalized mesoporous materials by the increase of the titanium content, Dalton Trans. 39 (2010) 2597–2608. https://doi.org/10.1039/b920051g.

[11] A. García-Peñas, S. Gómez-Ruiz, D. Pérez-Quintanilla, R. Paschke, I. Sierra, S. Prashar, I. del Hierro, G.N. Kaluđerović, Study of the cytotoxicity and particle action in human cancer cells of titanocene-functionalized materials with potential

application against tumors, J. Inorg. Biochem. 106 (2012) 100–110. https://doi.org/10.1016/j.jinorgbio.2011.09.033.

[12] J. Ceballos-Torres, P. Virag, M. Cenariu, S. Prashar, M. Fajardo, E. Fischer-Fodor, S. Gómez-Ruiz, Anti-cancer Applications of Titanocene-Functionalised Nanostructured Systems: An Insight into Cell Death Mechanisms, Chemistry – A European Journal. 20 (2014) 10811–10828. https://doi.org/10.1002/chem.201400300.

[13] J. Ceballos-Torres, S. Prashar, M. Fajardo, A. Chicca, J. Gertsch, A.B. Pinar, S. Gómez-Ruiz, Ether-Substituted Group 4 Metallocene Complexes: Cytostatic Effects and Applications in Ethylene Polymerization, Organometallics. 34 (2015) 2522–2532. https://doi.org/10.1021/om5012209.

[14] S. Gómez-Ruiz, A. García-Peñas, S. Prashar, A. Rodríguez-Diéguez, E. Fischer-Fodor, Anticancer Applications of Nanostructured Silica-Based Materials Functionalized with Titanocene Derivatives: Induction of Cell Death Mechanism through TNFR1 Modulation, Materials (Basel). 11 (2018) 224. https://doi.org/10.3390/ma11020224.

[15] D. Díaz-García, D. Cenariu, Y. Pérez, P. Cruz, I. del Hierro, S. Prashar, E. Fischer-Fodor, S. Gómez-Ruiz, Modulation of the mechanism of apoptosis in cancer cell lines by treatment with silica-based nanostructured materials functionalized with different metallodrugs, Dalton Trans. 47 (2018) 12284–12299. https://doi.org/10.1039/C8DT01677A.

[16] M.Z. Bulatović, D. Maksimović-Ivanić, C. Bensing, S. Gómez-Ruiz, D. Steinborn, H. Schmidt, M. Mojić, A. Korać, I. Golić, D. Pérez-Quintanilla, M. Momčilović, S. Mijatović, G.N. Kaluđerović, Organotin(IV)-loaded mesoporous silica as a biocompatible strategy in cancer treatment, Angew. Chem. Int. Ed. Engl. 53 (2014) 5982–5987. https://doi.org/10.1002/anie.201400763.

[17] C. Bensing, M. Mojić, S. Gómez-Ruiz, S. Carralero, B. Dojčinović, D. Maksimović-Ivanić, S. Mijatović, G.N. Kaluđerović, Evaluation of functionalized mesoporous silica

SBA-15 as a carrier system for Ph3Sn(CH2)3OH against the A2780 ovarian carcinoma cell line, Dalton Trans. 45 (2016) 18984–18993. https://doi.org/10.1039/c6dt03519a.

[18] D. Maksimović-Ivanić, M. Bulatović, D. Edeler, C. Bensing, I. Golić, A. Korać, G.N. Kaluđerović, S. Mijatović, The interaction between SBA-15 derivative loaded with Ph3Sn(CH2)6OH and human melanoma A375 cell line: uptake and stem phenotype loss, J Biol Inorg Chem. 24 (2019) 223–234. https://doi.org/10.1007/s00775-019-01640-x.

[19] D. Edeler, D. Drača, V. Petković, F. Natalio, D. Maksimović-Ivanić, S. Mijatović, H. Schmidt, G.N. Kaluđerović, Impact of the mesoporous silica SBA-15 functionalization on the mode of action of Ph3Sn(CH2)6OH, Materials Science and Engineering: C. 100 (2019) 315–322. https://doi.org/10.1016/j.msec.2019.03.010.

[20] Y. Ellahioui, M. Patra, C. Mari, R. Kaabi, J. Karges, G. Gasser, S. Gómez-Ruiz, Mesoporous silica nanoparticles functionalised with a photoactive ruthenium(ii) complex: exploring the formulation of a metal-based photodynamic therapy photosensitiser, Dalton Transactions. 48 (2019) 5940–5951. https://doi.org/10.1039/C8DT02392A.

[21] D. Díaz-García, P.R. Ardiles, S. Prashar, A. Rodríguez-Diéguez, P.L. Páez, S. Gómez-Ruiz, Preparation and Study of the Antibacterial Applications and Oxidative Stress Induction of Copper Maleamate-Functionalized Mesoporous Silica Nanoparticles, Pharmaceutics. 11 (2019) 30. https://doi.org/10.3390/pharmaceutics11010030.

[22] Y. Zhou, G. Quan, Q. Wu, X. Zhang, B. Niu, B. Wu, Y. Huang, X. Pan, C. Wu, Mesoporous silica nanoparticles for drug and gene delivery, Acta Pharmaceutica Sinica B. 8 (2018) 165–177. https://doi.org/10.1016/j.apsb.2018.01.007.

[23] S. Sánchez-Muñoz, S. Gómez-Ruiz, D. Pérez-Quintanilla, S. Morante-Zarcero, I. Sierra, S. Prashar, R. Paschke, G.N. Kaluđerović, Preliminary study of the anticancer

applications of mesoporous materials functionalized with the natural product betulinic acid, ChemMedChem. 7 (2012) 670–679. https://doi.org/10.1002/cmdc.201100588.

[24] S. Sapino, E. Ugazio, L. Gastaldi, I. Miletto, G. Berlier, D. Zonari, S. Oliaro-Bosso, Mesoporous silica as topical nanocarriers for quercetin: characterization and in vitro studies, European Journal of Pharmaceutics and Biopharmaceutics. 89 (2015) 116–125. https://doi.org/10.1016/j.ejpb.2014.11.022.

[25] V.S. Bollu, A.K. Barui, S.K. Mondal, S. Prashar, M. Fajardo, D. Briones, A. Rodríguez-Diéguez, C.R. Patra, S. Gómez-Ruiz, Curcumin-loaded silica-based mesoporous materials: Synthesis, characterization and cytotoxic properties against cancer cells, Mater Sci Eng C Mater Biol Appl. 63 (2016) 393–410. https://doi.org/10.1016/j.msec.2016.03.011.

[26] R. Kotcherlakota, A.K. Barui, S. Prashar, M. Fajardo, D. Briones, A. Rodríguez-Diéguez, C.R. Patra, S. Gómez-Ruiz, Curcumin loaded mesoporous silica: an effective drug delivery system for cancer treatment, Biomater. Sci. 4 (2016) 448–459. https://doi.org/10.1039/C5BM00552C.

[27] T.L. Nguyen, Y. Choi, J. Kim, Mesoporous Silica as a Versatile Platform for Cancer Immunotherapy, Advanced Materials. in press (2019) 1803953. https://doi.org/10.1002/adma.201803953.

[28] P.V. Baptista, M.P. McCusker, A. Carvalho, D.A. Ferreira, N.M. Mohan, M. Martins, A.R. Fernandes, Nano-Strategies to Fight Multidrug Resistant Bacteria—"A Battle of the Titans," Front Microbiol. 9 (2018). https://doi.org/10.3389/fmicb.2018.01441.

[29] M. Martínez-Carmona, Y.K. Gun'ko, M. Vallet-Regí, Mesoporous Silica Materials as Drug Delivery: "The Nightmare" of Bacterial Infection, Pharmaceutics. 10 (2018) 279. https://doi.org/10.3390/pharmaceutics10040279.

[30] L. Rizzello, R. Cingolani, P.P. Pompa, Nanotechnology tools for antibacterial materials, Nanomedicine. 8 (2013) 807–821. https://doi.org/10.2217/nnm.13.63.

[31] Z. Gounani, M.A. Asadollahi, Jannik.N. Pedersen, J. Lyngsø, J. Skov Pedersen, A. Arpanaei, R.L. Meyer, Mesoporous silica nanoparticles carrying multiple antibiotics

provide enhanced synergistic effect and improved biocompatibility, Colloids and Surfaces B: Biointerfaces. 175 (2019) 498–508. https://doi.org/10.1016/j.colsurfb.2018.12.035.

[32] B. González, M. Colilla, J. Díez, D. Pedraza, M. Guembe, I. Izquierdo-Barba, M. Vallet-Regí, Mesoporous silica nanoparticles decorated with polycationic dendrimers for infection treatment, Acta Biomaterialia. 68 (2018) 261–271. https://doi.org/10.1016/j.actbio.2017.12.041.

[33] M. Michailidis, I. Sorzabal-Bellido, E.A. Adamidou, Y.A. Diaz-Fernandez, J. Aveyard, R. Wengier, D. Grigoriev, R. Raval, Y. Benayahu, R.A. D'Sa, D. Shchukin, Modified Mesoporous Silica Nanoparticles with a Dual Synergetic Antibacterial Effect, ACS Appl. Mater. Interfaces. 9 (2017) 38364–38372. https://doi.org/10.1021/acsami.7b14642.

[34] Y. Tian, J. Qi, W. Zhang, Q. Cai, X. Jiang, Facile, One-Pot Synthesis, and Antibacterial Activity of Mesoporous Silica Nanoparticles Decorated with Well-Dispersed Silver Nanoparticles, ACS Appl. Mater. Interfaces. 6 (2014) 12038–12045. https://doi.org/10.1021/am5026424.

[35] L. Tahmasbi, T. Sedaghat, H. Motamedi, M. Kooti, Mesoporous silica nanoparticles supported copper(II) and nickel(II) Schiff base complexes: Synthesis, characterization, antibacterial activity and enzyme immobilization, Journal of Solid State Chemistry. 258 (2018) 517–525. https://doi.org/10.1016/j.jssc.2017.11.015.

[36] K.N. Lazarou, I. Chadjistamatis, V. Psycharis, S.P. Perlepes, C.P. Raptopoulou, First use of the maleamate(−1) ligand in coordination chemistry: Dinuclear copper(II) complexes with N-donors and their interesting 'organic' chemistry, Inorganic Chemistry Communications. 10 (2007) 318–323. https://doi.org/10.1016/j.inoche.2006.11.006.

[37] K.N. Lazarou, S.P. Perlepes, V. Psycharis, C.P. Raptopoulou, Synthetic study of the ternary copper(II)/maleamate(-1)/1,10-phenanthroline reaction system:

Mononuclear, dinuclear and polymeric complexes, Polyhedron. 27 (2008) 2131–2142. https://doi.org/10.1016/j.poly.2008.04.005.

[38] K.N. Lazarou, V. Psycharis, S.P. Perlepes, C.P. Raptopoulou, Complexes derived from the copper(II) perchlorate/maleamic acid/2,2′-bipyridine and copper(II) perchlorate/maleic acid/2,2′-bipyridine reaction systems: Synthetic, reactivity, structural and spectroscopic studies, Polyhedron. 28 (2009) 1085–1096. https://doi.org/10.1016/j.poly.2009.01.023.

[39] K.N. Lazarou, A.K. Boudalis, S.P. Perlepes, A. Terzis, C.P. Raptopoulou, Maleamate(–1) and Maleate(–2) Copper(II)–2,2′-Bipyridine Complexes: Synthesis, Reactivity and Structural and Physical Studies, European Journal of Inorganic Chemistry. 2009 (2009) 4554–4563. https://doi.org/10.1002/ejic.200900485.

[40] K.N. Lazarou, C.P. Raptopoulou, S.P. Perlepes, V. Psycharis, Complexes derived from the general copper(II)/maleamic acid/N,N′,N″-chelate reaction systems: Synthetic, reactivity, structural and spectroscopic studies, Polyhedron. 28 (2009) 3185–3192. https://doi.org/10.1016/j.poly.2009.04.016.

[41] V.A. Kincaid, E.D. Sullivan, R.D. Klein, J.W. Noel, R.S. Rowlett, M.J. Snider, Structure and Catalytic Mechanism of Nicotinate (Vitamin B3) Degradative Enzyme Maleamate Amidohydrolase from Bordetella bronchiseptica RB50, Biochemistry. 51 (2012) 545–554. https://doi.org/10.1021/bi201347n.

[42] R.C.F. Burdon, R.R. Junker, D.G. Scofield, A.L. Parachnowitsch, Bacteria colonising Penstemon digitalis show volatile and tissue-specific responses to a natural concentration range of the floral volatile linalool, Chemoecology. 28 (2018) 11–19. https://doi.org/10.1007/s00049-018-0252-x.

[43] U. Brahma, R. Kothari, P. Sharma, V. Bhandari, Antimicrobial and anti-biofilm activity of hexadentated macrocyclic complex of copper (II) derived from thiosemicarbazide against Staphylococcus aureus, Scientific Reports. 8 (2018) 8050. https://doi.org/10.1038/s41598-018-26483-5.

[44] S. Balakrishnan, S. Duraisamy, M. Kasi, S. Kandasamy, R. Sarkar, A. Kumarasamy, Syntheses, physicochemical characterization, antibacterial studies on potassium morpholine dithiocarbamate nickel (II), copper (II) metal complexes and their ligands, Heliyon. 5 (2019) e01687. https://doi.org/10.1016/j.heliyon.2019.e01687.

[45] K. Ohui, E. Afanasenko, F. Bacher, R.L.X. Ting, A. Zafar, N. Blanco-Cabra, E. Torrents, O. Dömötör, N.V. May, D. Darvasiova, É.A. Enyedy, A. Popović-Bijelić, J. Reynisson, P. Rapta, M.V. Babak, G. Pastorin, V.B. Arion, New Water-Soluble Copper(II) Complexes with Morpholine–Thiosemicarbazone Hybrids: Insights into the Anticancer and Antibacterial Mode of Action, J. Med. Chem. 62 (2019) 512–530. https://doi.org/10.1021/acs.jmedchem.8b01031.

[46] N. Rani, A. Sharma, R. Singh, Imidazoles as promising scaffolds for antibacterial activity: a review, Mini Rev Med Chem. 13 (2013) 1812–1835.

[47] L.X. Zhang, X.-M. Peng, G.L.V. Damu, R.H. Geng, C.-H. Zhou, Comprehensive review in current developments of imidazole-based medicinal chemistry., Medicinal Research Reviews. 34 (2014) 340–437. https://doi.org/10.1002/med.21290.

[48] A. Lewis, M. McDonald, S. Scharbach, S. Hamaway, M. Plooster, K. Peters, K.M. Fox, L. Cassimeris, J.M. Tanski, L.A. Tyler, The chemical biology of Cu(II) complexes with imidazole or thiazole containing ligands: Synthesis, crystal structures and comparative biological activity, J. Inorg. Biochem. 157 (2016) 52–61. https://doi.org/10.1016/j.jinorgbio.2016.01.014.

[49] K. Gałczyńska, K. Ciepluch, Ł. Madej, K. Kurdziel, B. Maciejewska, Z. Drulis-Kawa, A. Węgierek-Ciuk, A. Lankoff, M. Arabski, Selective cytotoxicity and antifungal properties of copper(II) and cobalt(II) complexes with imidazole-4-acetate anion or 1-allylimidazole, Scientific Reports. 9 (2019) 9777. https://doi.org/10.1038/s41598-019-46224-6.

[50] A. Typas, M. Banzhaf, C.A. Gross, W. Vollmer, From the regulation of peptidoglycan synthesis to bacterial growth and morphology, Nature Reviews Microbiology. 10 (2012) 123–136. https://doi.org/10.1038/nrmicro2677.

[51] D. Zhao, J. Sun, Q. Li, G.D. Stucky, Morphological Control of Highly Ordered Mesoporous Silica SBA-15, Chem. Mater. 12 (2000) 275–279. https://doi.org/10.1021/cm9911363.

[52] CLSI (Clinical and Laboratory Standards Institute), Methods for Dilution Antimicrobial Susceptibility Tests for Bacteria That Grow Aerobically. Approved Standard, M07-A8. 8. CLSI, Wayne, PA, USA., (2011).

[53] M. Thommes, K. Kaneko, A.V. Neimark, J.P. Olivier, F. Rodriguez-Reinoso, J. Rouquerol, K.S.W. Sing, Physisorption of gases, with special reference to the evaluation of surface area and pore size distribution (IUPAC Technical Report), Pure and Applied Chemistry. 87 (2015) 1051–1069. https://doi.org/10.1515/pac-2014-1117.

[54] X.S. Zhao, G.Q. Lu, A.K. Whittaker, G.J. Millar, H.Y. Zhu, Comprehensive Study of Surface Chemistry of MCM-41 Using 29Si CP/MAS NMR, FTIR, Pyridine-TPD, and TGA, J. Phys. Chem. B. 101 (1997) 6525–6531. https://doi.org/10.1021/jp971366+.

[55] C. Wang, H. Zhou, H. Niu, X. Ma, Y. Yuan, H. Hong, C. Liu, Tannic acid-loaded mesoporous silica for rapid hemostasis and antibacterial activity, Biomater. Sci. 6 (2018) 3318–3331. https://doi.org/10.1039/C8BM00837J.

[56] P.L. Páez, C.M. Bazán, M.E. Bongiovanni, J. Toneatto, I. Albesa, M.C. Becerra, G.A. Argüello, Oxidative stress and antimicrobial activity of chromium(III) and ruthenium(II) complexes on Staphylococcus aureus and Escherichia coli, Biomed Res Int. 2013 (2013) 906912. https://doi.org/10.1155/2013/906912.

[57] B. Matynia, E. Młodzinska, W. Hryniewicz, Antimicrobial susceptibility patterns of Staphylococcus aureus in Poland obtained by the National Quality Assurance Programme, Clin. Microbiol. Infect. 11 (2005) 379–385. https://doi.org/10.1111/j.1469-0691.2005.01105.x.

[58] E. Domínguez, M. Zarazaga, Y. Sáenz, L. Briñas, C. Torres, Mechanisms of antibiotic resistance in Escherichia coli isolates obtained from healthy children in

Spain, Microb. Drug Resist. 8 (2002) 321–327. https://doi.org/10.1089/10766290260469589.

[59] M.A. Quinteros, V. Cano Aristizábal, P.R. Dalmasso, M.G. Paraje, P.L. Páez, Oxidative stress generation of silver nanoparticles in three bacterial genera and its relationship with the antimicrobial activity, Toxicol In Vitro. 36 (2016) 216–223. https://doi.org/10.1016/j.tiv.2016.08.007.

[60] N. Durán, M. Durán, M.B. de Jesus, A.B. Seabra, W.J. Fávaro, G. Nakazato, Silver nanoparticles: A new view on mechanistic aspects on antimicrobial activity, Nanomedicine: Nanotechnology, Biology and Medicine. 12 (2016) 789–799. https://doi.org/10.1016/j.nano.2015.11.016.

[61] C.R. Kowol, P. Heffeter, W. Miklos, L. Gille, R. Trondl, L. Cappellacci, W. Berger, B.K. Keppler, Mechanisms underlying reductant-induced reactive oxygen species formation by anticancer copper(II) compounds, J. Biol. Inorg. Chem. 17 (2012) 409–423. https://doi.org/10.1007/s00775-011-0864-x.

[62] M.K. Lesiów, U.K. Komarnicka, K. Stokowa-Sołtys, K. Rolka, A. Łęgowska, N. Ptaszyńska, R. Wieczorek, A. Kyzioł, M. Jeżowska-Bojczuk, Relationship between copper(II) complexes with FomA adhesin fragments of F. nucleatum and colorectal cancer. Coordination pattern and ability to promote ROS production, Dalton Trans. 47 (2018) 5445–5458. https://doi.org/10.1039/C7DT04103A.

[63] M. Cavicchioli, A.M.L. Zaballa, Q.A. de Paula, M.B. Prieto, C.C. Oliveira, P. Civitareale, M.R. Ciriolo, A.M. Da Costa Ferreira, Oxidative Assets Toward Biomolecules and Cytotoxicity of New Oxindolimine-Copper(II) and Zinc(II) Complexes, Inorganics. 7 (2019) 12. https://doi.org/10.3390/inorganics7020012.

[64] D.-J. Scheffers, M.G. Pinho, Bacterial Cell Wall Synthesis: New Insights from Localization Studies, Microbiol Mol Biol Rev. 69 (2005) 585–607. https://doi.org/10.1128/MMBR.69.4.585-607.2005.

[65] H. Suzuki, W. Hashimoto, H. Kumagai, Glutathione metabolism in Escherichia coli, Journal of Molecular Catalysis B: Enzymatic. 6 (1999) 175–184. https://doi.org/10.1016/S1381-1177(98)00116-7.

[66] G.P. Ferguson, I.R. Booth, Importance of Glutathione for Growth and Survival of Escherichia coli Cells: Detoxification of Methylglyoxal and Maintenance of Intracellular K+, Journal of Bacteriology. 180 (1998) 4314–4318.

[67] J. Zhang, C. Quan, C. Wang, H. Wu, Z. Li, Q. Ye, Systematic manipulation of glutathione metabolism in Escherichia coli for improved glutathione production, Microb Cell Fact. 15 (2016). https://doi.org/10.1186/s12934-016-0439-1.

[68] D.O. Schairer, J.S. Chouake, A.J. Kutner, J. Makdisi, J.D. Nosanchuk, A.J. Friedman, Evaluation of the antibiotic properties of glutathione, J Drugs Dermatol. 12 (2013) 1272–1277.

[69] Y. Zhang, K. Duan, Glutathione exhibits antibacterial activity and increases tetracycline efficacy against Pseudomonas aeruginosa, Sci. China, C, Life Sci. 52 (2009) 501–505. https://doi.org/10.1007/s11427-009-0074-8.

[70] R. Alharbe, A. Almansour, D.H. Kwon, Antibacterial activity of exogenous glutathione and its synergism on antibiotics sensitize carbapenem-associated multidrug resistant clinical isolates of Acinetobacter baumannii, International Journal of Medical Microbiology. 307 (2017) 409–414. https://doi.org/10.1016/j.ijmm.2017.07.009.

[71] P.A.M. Farias, M.B.R. Bastos, Electrochemical Behavior of Copper(II) salen in Aqueous Phosphate Buffer at the Mercury Electrode, Int. J. Electrochem. Sci. 4 (2009) 13.

[72] M. Mureseanu, D.E. Popa, M. Buleandră, I. Trandafir, N. Cioateră, D. Şendrescu, I. Tănase, Copper Electrochemical Detection with Hybrid Mesoporous Silica-Gly-Gly-His Modified Electrodes, Int. J. Electrochem. Sci. 9 (2014) 14.

[73] M.I. Rodríguez, T. Chávez-Gil, Y. Colón, N. Díaz, E. Meléndez, Molybdenocene–DNA interaction studies using electrochemical analysis, Journal of Electroanalytical Chemistry. 576 (2005) 315–322. https://doi.org/10.1016/j.jelechem.2004.11.005.

[74] I. Feliciano, J. Matta, E. Meléndez, Water-soluble molybdenocene complexes with both proliferative and antiproliferative effects on cancer cell lines and their binding interactions with human serum albumin, J Biol Inorg Chem. 14 (2009) 1109–1117. https://doi.org/10.1007/s00775-009-0554-0.

[75] A.J. Santiago-Lopez, J.L. Vera, E. Meléndez, DNA electrochemical biosensor for metallic drugs at physiological conditions, Journal of Electroanalytical Chemistry. 731 (2014) 139–144. https://doi.org/10.1016/j.jelechem.2014.07.022.

[76] S.A. Lahsasni, R.A. Ammar, M.F. Amin, E.M. Shoukry, Mixed-Ligand Complex Formation of Cu(II) with 1,2- Diphenylethylenediamine as Primary Ligand and Amino Acids as Secondary Ligands, Int. J. Electrochem. Sci. 7 (2012) 13.

[77] H. Aliyu, J. Na'aliya, Potentiometric studies on essential metal (II) amino acid complexes, in: 2012.

[78] B.C. Khade, P.M. Deore, B.R. Arbad, Mixed-ligand complex formation of copper (II) with some aminoacids and Drug Dapsone, in: 2003.

[79] Y.Z. Hamada, N.J. Makoni, H. Hamada, Cu2+ Complexes with the Simplest Amino Acid Glycine (Gly), in: 2017. https://doi.org/10.15406/jnmr.2017.05.00123.

Figures and Schemes

Figure 1. XRD diffraction patterns of SBA-15, SBA-maleamic and SBA-maleamic-Cu

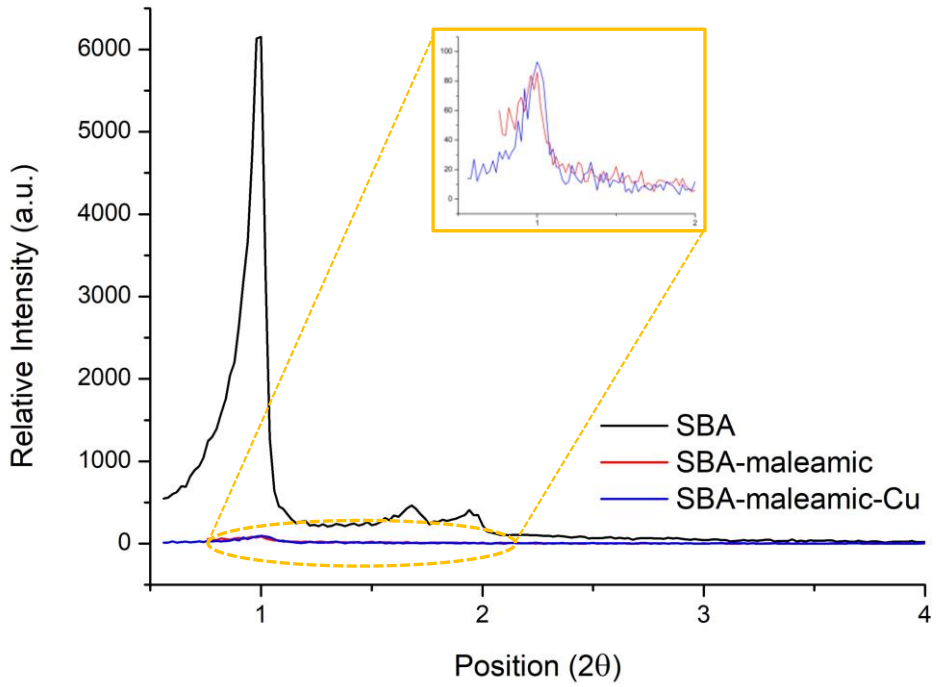

Figure 2. Nitrogen adsorption/desorption isotherms of SBA-15, SBA-maleamic-Cu and SBA-imidazoline-Cu

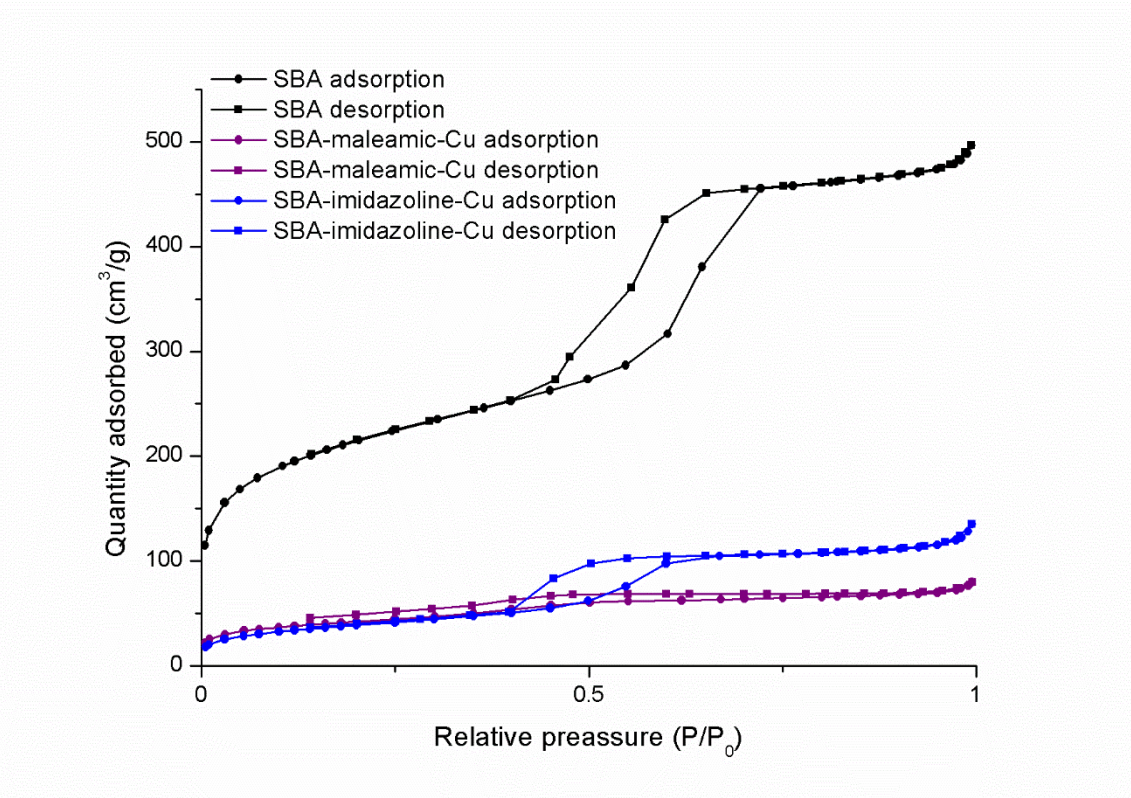

Figure 3. SEM and TEM images of unmodified SBA-15

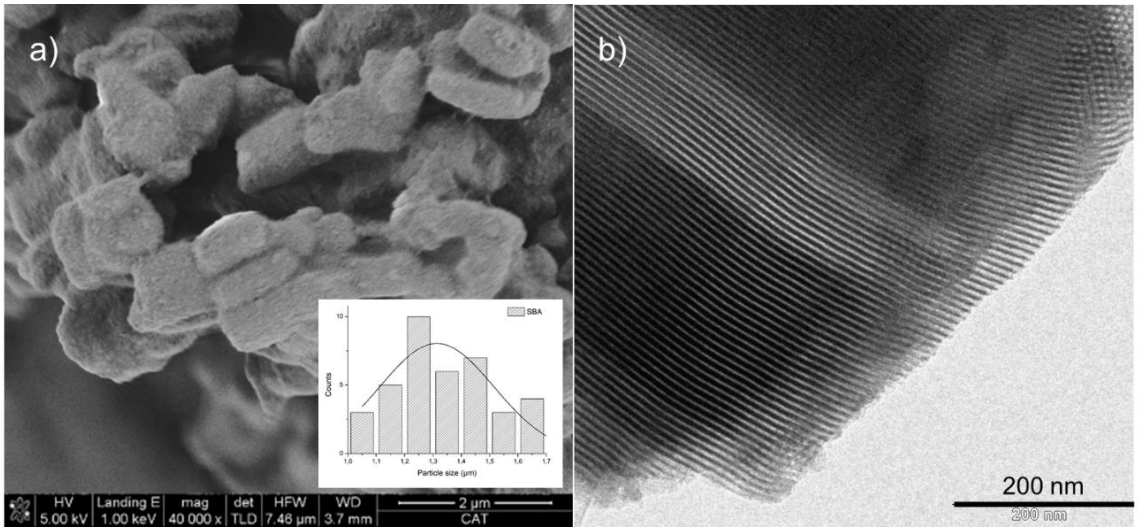

Figure 4. ^{29}Si MAS NMR spectra of SBA-15, SBA-maleamic, SBA-maleamic-Cu, SBA-imidazoline and SBA-imidazoline-Cu

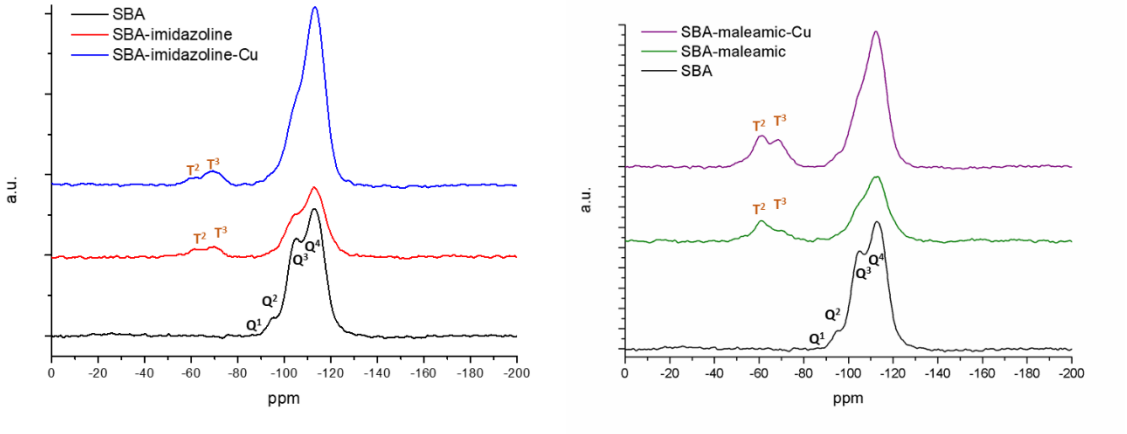

Figure 5. ^{13}C CP MAS NMR spectra of SBA-maleamic-Cu (up) and SBA-imidazoline-Cu (down)

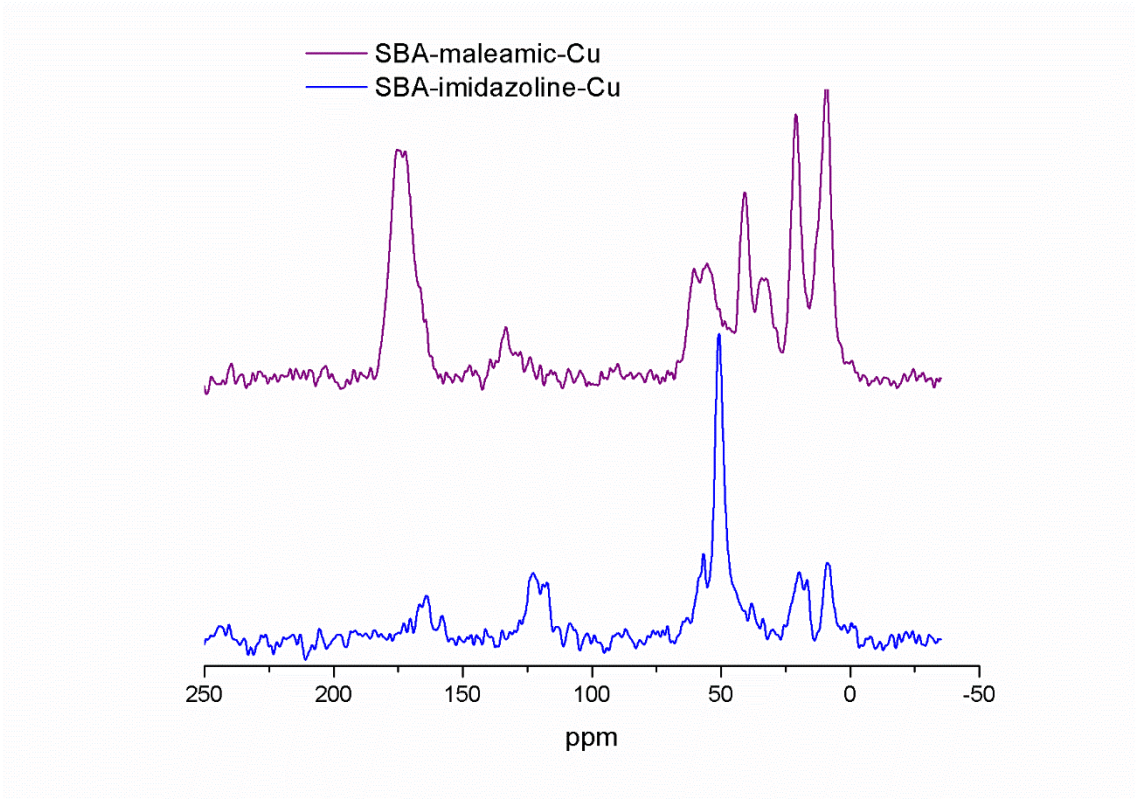

Figure 6. DR-UV spectra of a) SBA-maleamic and SBA-maleamic-Cu and b) SBA-imidazoline and SBA-imidazoline-Cu

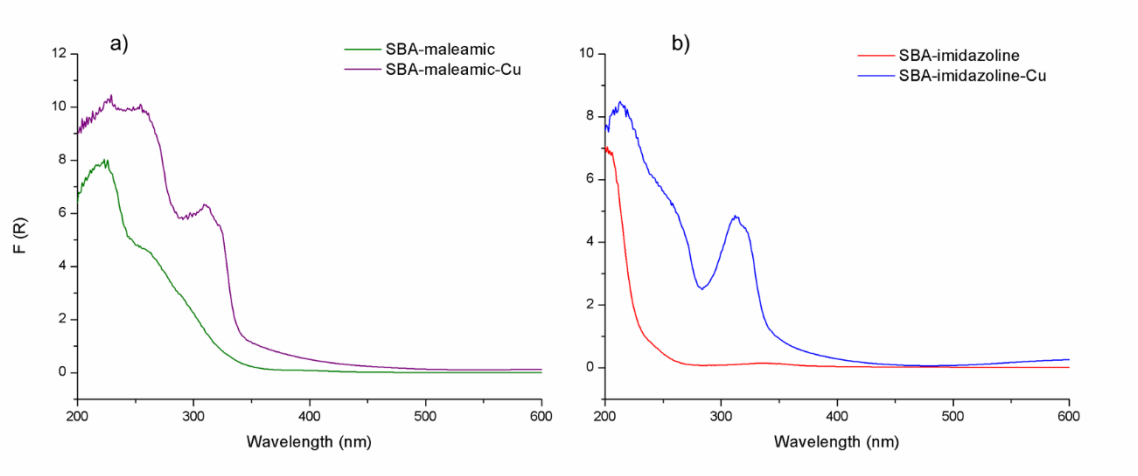

Figure 7. SEM images of a) SBA-15-maleamic-Cu and b) SBA-15-imidazoline-Cu

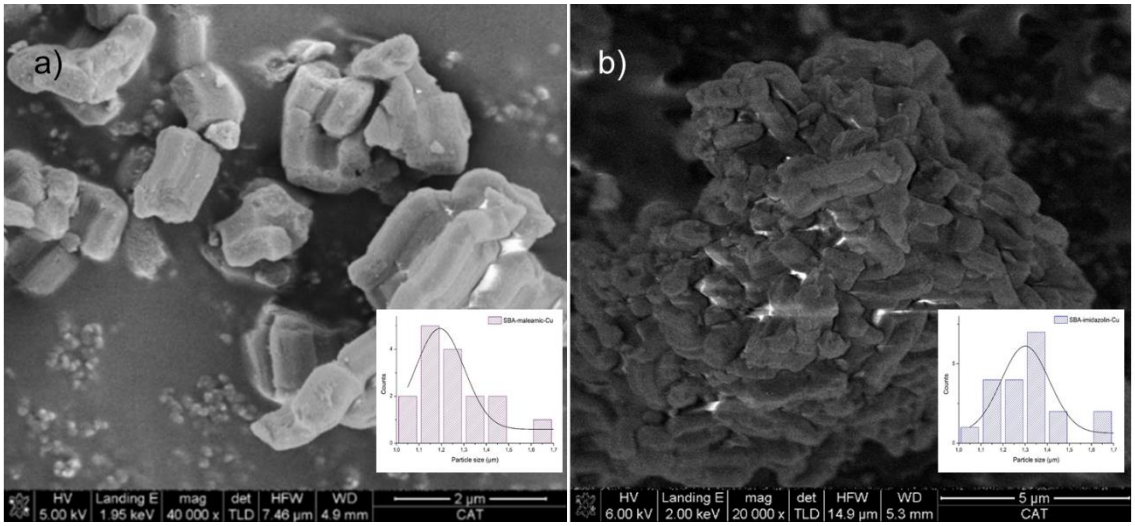

Figure 8. EDX mapping of a SEM image of SBA-imidazoline-Cu showing the distribution of Si, O and Cu atoms on the external surface area of the material.

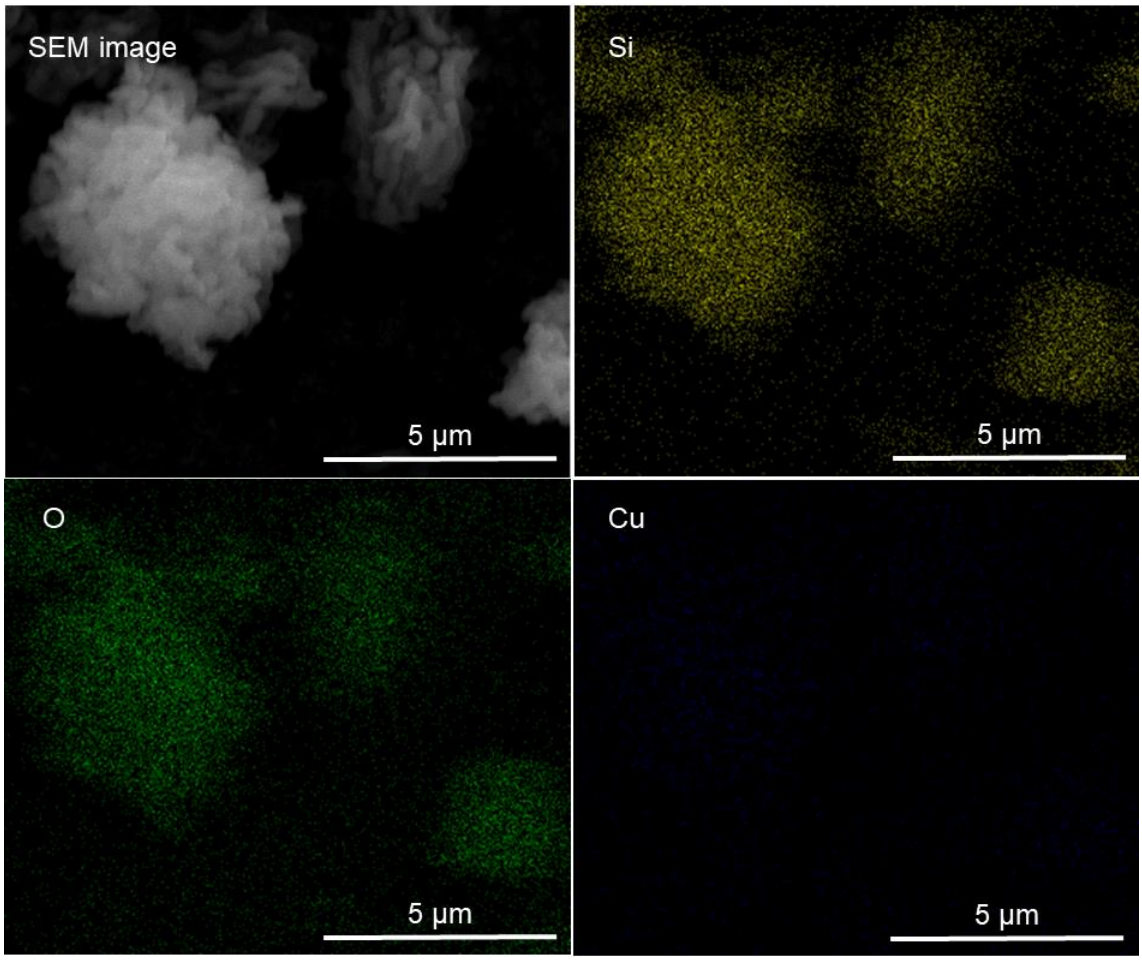

Figure 9. TEM images of a) SBA-15 maleamic-Cu and b) SBA-15-imidazoline-Cu

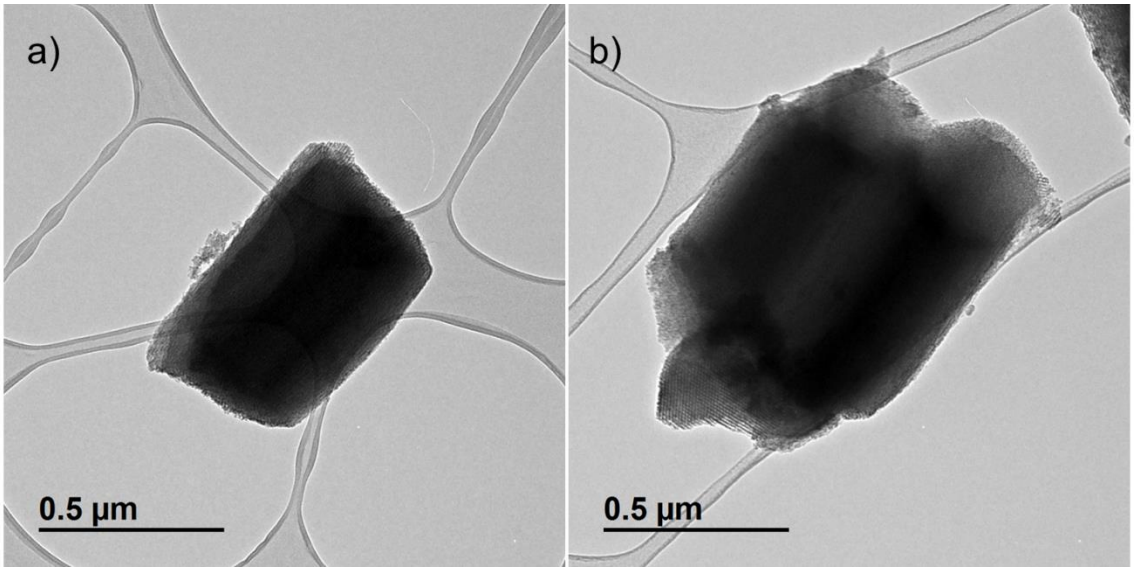

Figure 10. Percentage reactive oxygen species (ROS) increase induced in bacterial suspensions incubated with 100 µL of the synthesized materials SBA-15, SBA-maleamic, SBA-maleamic-Cu, SBA-imidazoline and SBA-imidazoline-Cu at MIC (the study was carried out in triplicate the assays were performed at least in triplicate and data are expressed as means ±SD and analyzed by the Student's t-test. *p<0.05 respect to control and #p<0.05 respect to the complex without copper)

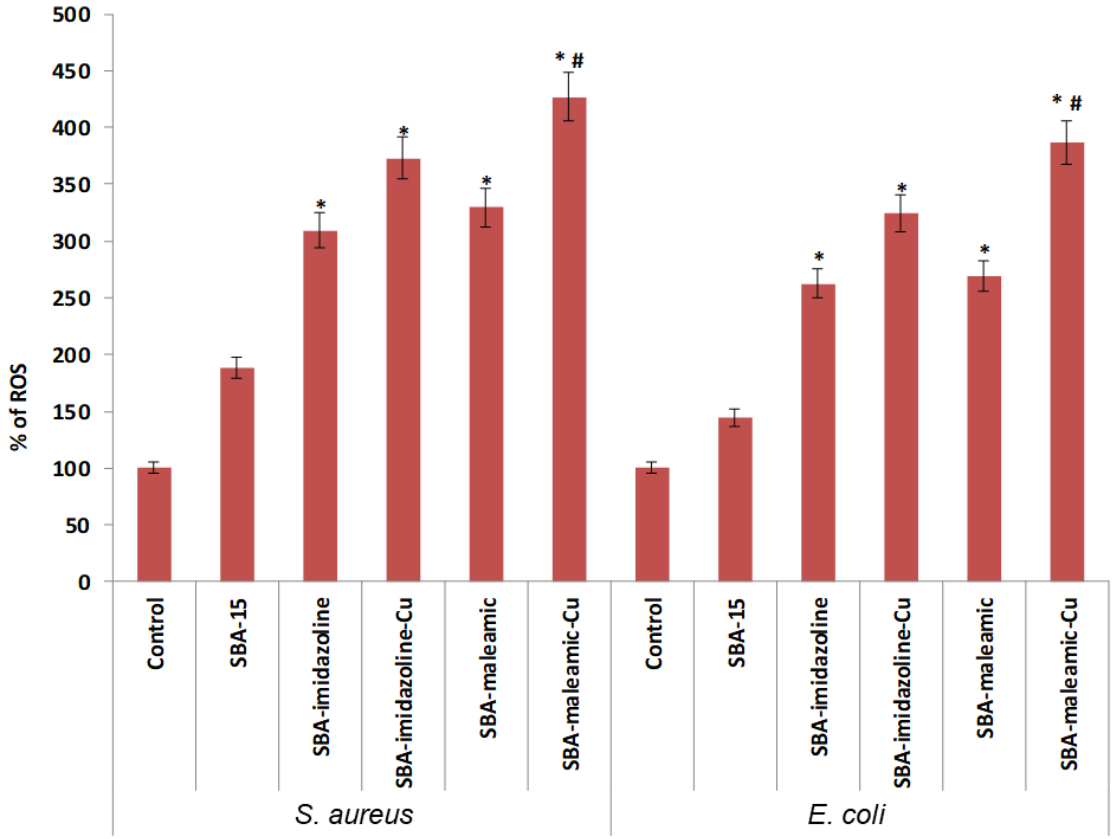

Figure 11. Cyclic voltammogram of SBA-maleamic-Cu carbon paste modified electrode in buffer phosphate at PH 7,4 *vs* Ag/AgCl,KCl(3M) scanned from +1.0 to -1.5V (scan speed from 10 to 500 mV/s)

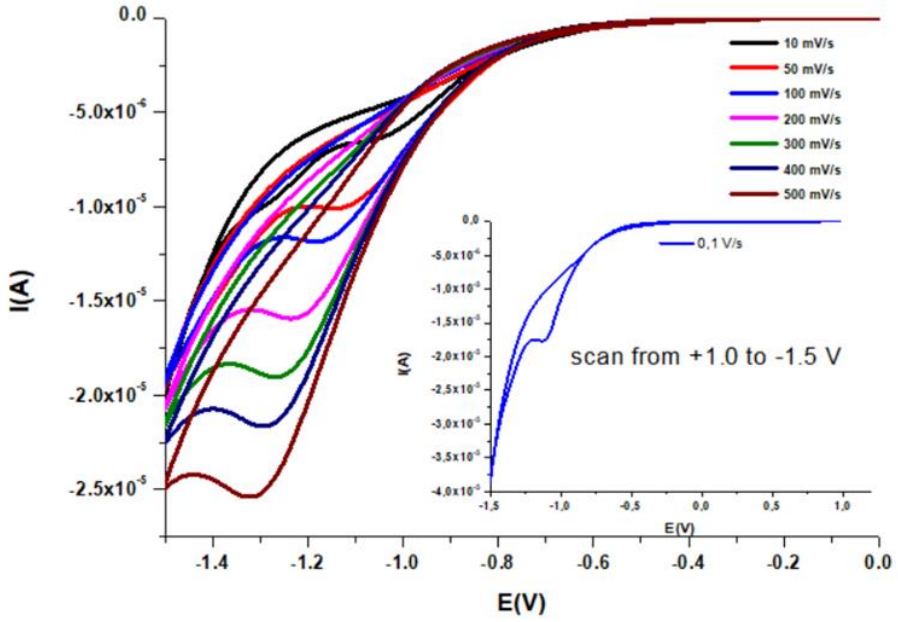

Figure 12. Differential pulse voltammogram of SBA-maleamic-Cu carbon paste modified electrode in buffer phosphate at pH 7.4 *vs* Ag/AgCl,KCl (3M) (scanned from +1.0 to -1.5V) and in the presence of lysine (A) 4, (B) 2 and (C) 0.5 mM

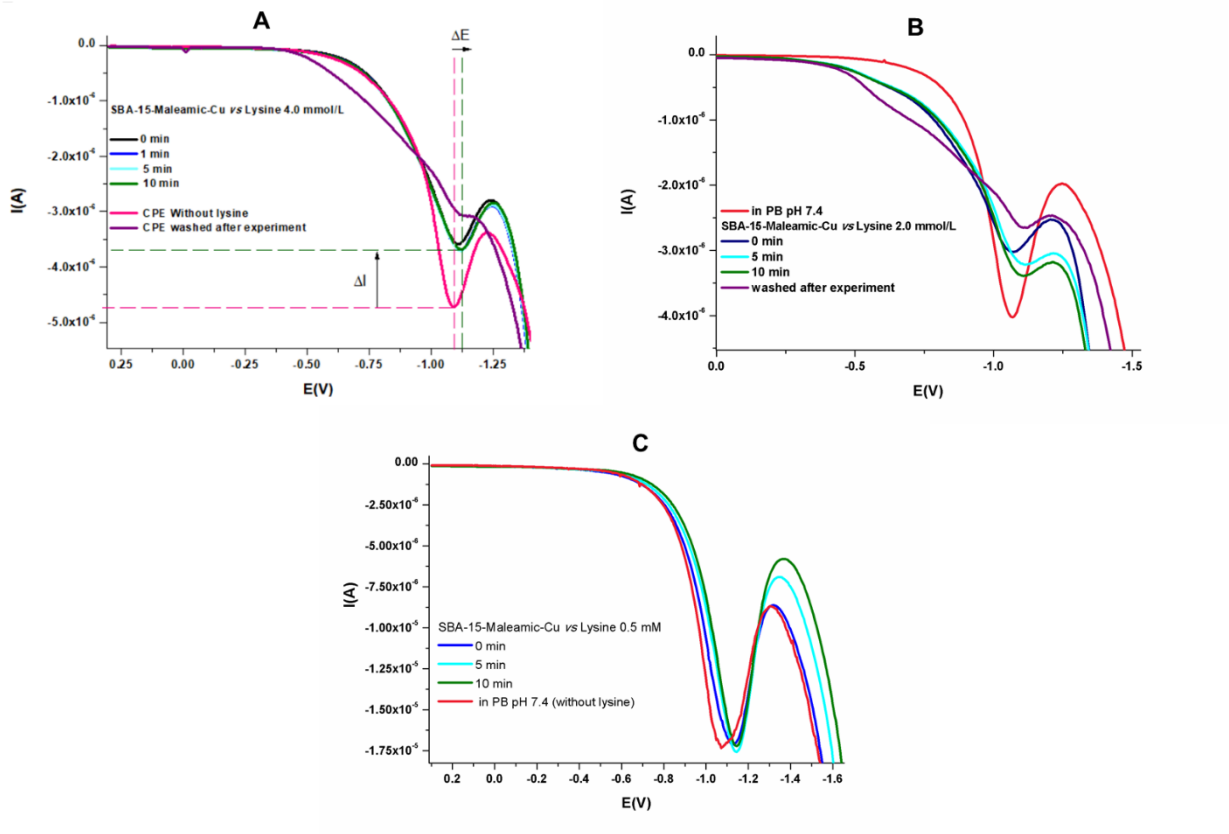

Scheme 1. Synthesis of a) SBA-maleamic and b) SBA-imidazoline

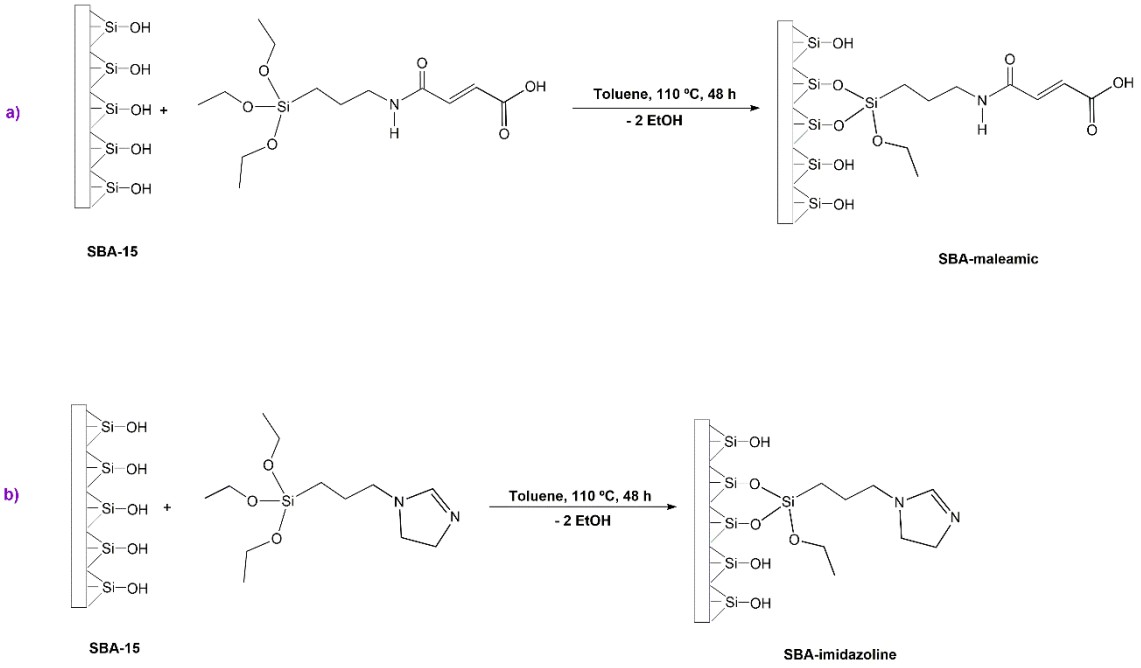

Scheme 2. Synthesis of a) SBA-maleamic-Cu and b) SBA-imidazoline-Cu

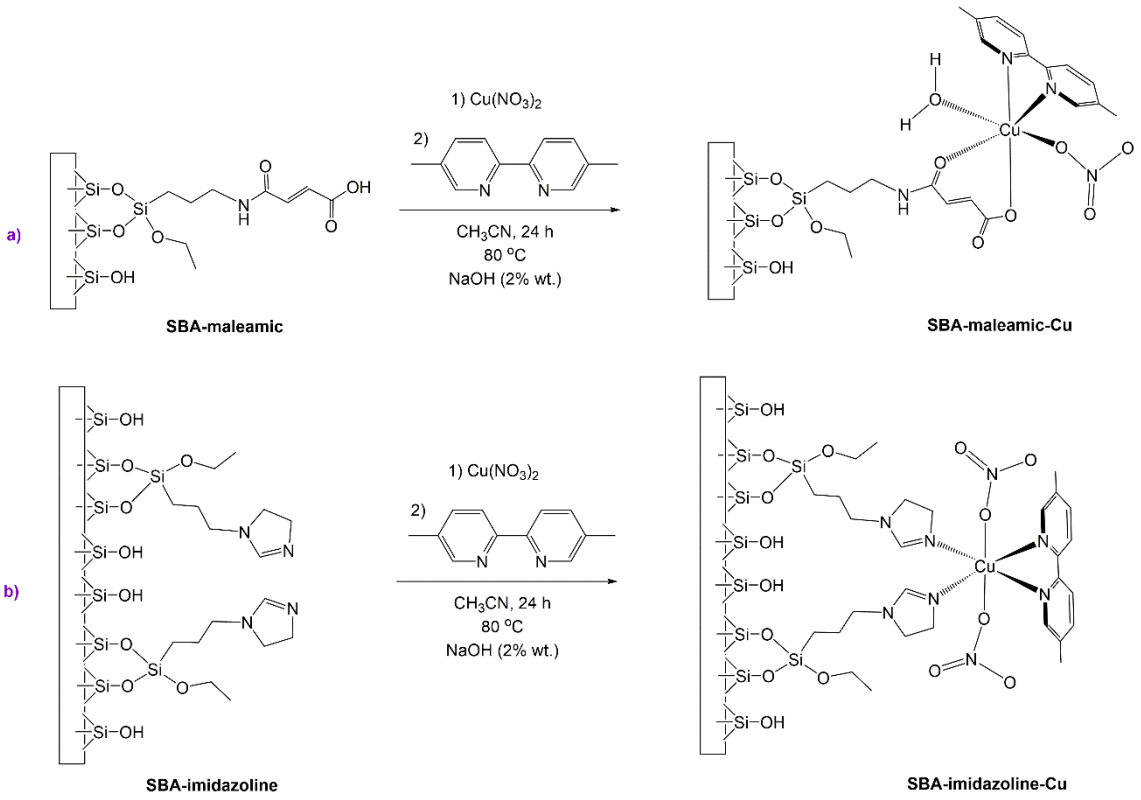

Scheme 3. Decoordination of bipyridine and formation of a copper complex of the type [Cu(lysine)$_2$] upon reaction of the copper-modified material SBA-maleamic-Cu with alanine in solution.

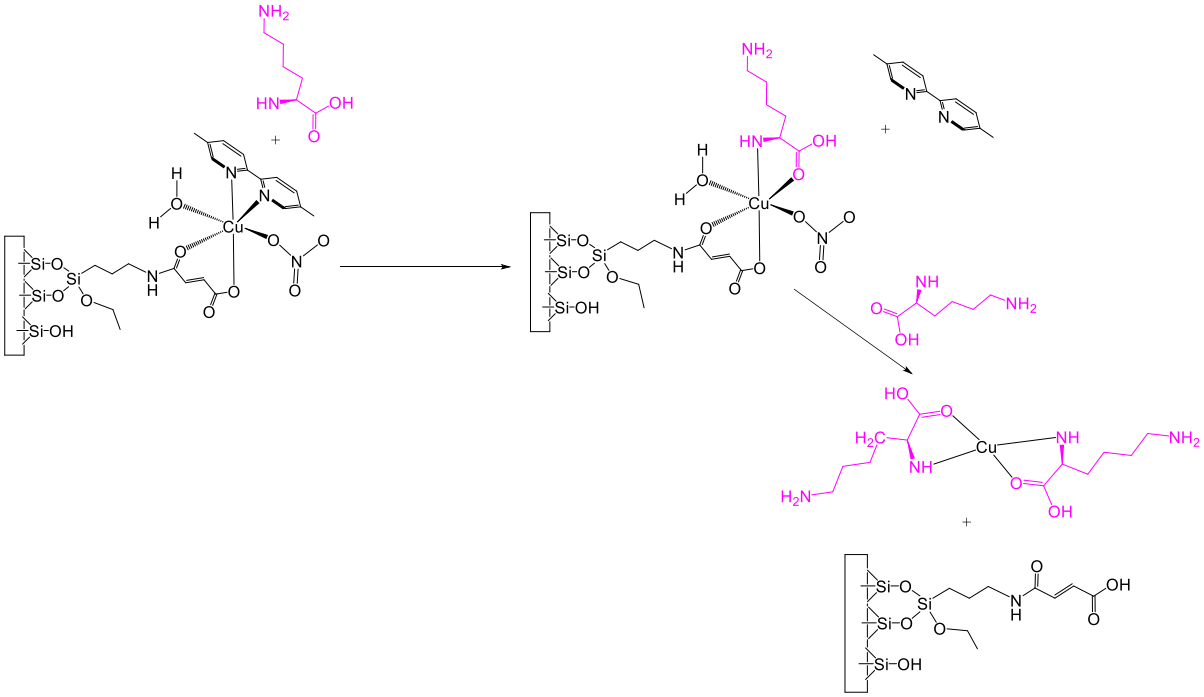

Tables

Table 1. XRD data of SBA-15, SBA-maleamic, SBA-maleamic-Cu, SBA-imidazoline and SBA-imidazoline-Cu

Material	*(hkl)*	2Θ(˚)	d_{hkl}(Å)	a_o(Å)
SBA-15	100	0.989	89.292	103.106
	110	1.688	52.343	
	200	1.957	45.139	
SBA-maleamic	100	0.986	89.514	103.362
SBA-maleamic-Cu	100	1.012	87.186	100.674
SBA-imidazoline	100	1.063	83.137	95.998
	110	2.026	43.615	
SBA-imidazoline-Cu	100	1.085	81.391	93.982
	110	2.041	43.277	

Table 2. Textural parameters (determined by nitrogen adsorption-desorption isotherms) and quantity of Cu (determined by XRF) of SBA-15, SBA-maleamic-Cu and SBA-imidazoline-Cu

Material	BET Surface (m^2/g)	Pore Volume (cm^3/g)	Pore Diameter (nm)	% Cu (Determined by XRF)	mmol Cu / gram of material
SBA-15	763	0.74	6.55		
SBA-maleamic-Cu	150	0.11	3.15	3.6	0.56
SBA-imidazoline-Cu	142	0.18	4.71	12.3	1.94

Table 3. Minimal inhibitory concentration (MIC) and minimal bactericidal concentration (MBC) values of SBA-15, SBA-maleamic, SBA-maleamic-Cu, SBA-imidazoline and SBA-imidazoline-Cu against *Staphylococcus aureus* and *Escherichia coli*. Data in brackets refer to MIC or MBC values in µg/mL of Cu.

Material / Bacteria	***Staphylococcus aureus* ATCC 29213**		***Escherichia coli* ATCC 25922**	
	MIC µg/mL	MBC µg/mL	MIC µg/mL	MBC µg/mL
SBA-15	>250	>250	>250	>250
SBA-maleamic	125	250	125	125
SBA-maleamic-Cu	31.25 [1.13]	62.5 [2.26]	31.25 [1.13]	31.25 [1.13]
SBA-imidazoline	125	125	62.5	62.5
SBA-imidazoline-Cu	62.5 [7.69]	125 [15.38]	31.25 [3.85]	62.5 [7.69]

Table 4. Change in potential (a) and current (b) for the electrochemical interaction of SBA-15-Maleamic-Cu vs Lysine, Alanine and Glutathione after surface electrode saturation (5 minutes time) in aqueous phosphate buffer pH 7.4

	Concentration (mM)	**% ΔI**	**% ΔE**
Lysine	4	47	3.2
	2	53	5.0
	1	35	3.2
	0.5	4	4.4
Alanine	2	47	2.3
	1	44	2.5
	0.5	21	0.7
Glutathione	2	33	0.2
	1	43	1.5
	0.5	6	0.2